

DISCOVERING SYMBOLIC DIFFERENTIAL EQUATIONS WITH SYMMETRY INVARIANTS

000
001
002
003
004
005
006
007
008
009
010
011
012
013
014
015
016
017
018
019
020
021
022
023
024
025
026
027
028
029
030
031
032
033
034
035
036
037
038
039
040
041
042
043
044
045
046
047
048
049
050
051
052
053
Anonymous authors
Paper under double-blind review

ABSTRACT

Discovering symbolic differential equations from data uncovers fundamental dynamical laws underlying complex systems. However, existing methods often struggle with the vast search space of equations and may produce equations that violate known physical laws. In this work, we address these problems by introducing the concept of *symmetry invariants* in equation discovery. We leverage the fact that differential equations admitting a symmetry group can be expressed in terms of differential invariants of symmetry transformations. Thus, we propose using these invariants as atomic entities in equation discovery, ensuring the discovered equations satisfy the specified symmetry. Our approach integrates seamlessly with existing equation discovery methods such as sparse regression and genetic programming, improving their accuracy and efficiency. We validate the proposed method through applications to various physical systems, such as Darcy flow and reaction-diffusion, demonstrating its ability to recover parsimonious and interpretable equations that respect the laws of physics.

1 INTRODUCTION

Differential equations describe relationships between functions representing physical quantities and their derivatives. They are crucial in modeling a wide range of phenomena, from fluid dynamics and electromagnetic fields to chemical reactions and biological processes, as they succinctly capture the underlying principles governing the behavior of complex systems. The discovery of governing equations in symbolic forms from observational data bridges the gap between raw data and fundamental understanding of physical systems. Unlike black-box machine learning models, symbolic equations provide interpretable insights into the structure and dynamics of the systems of interest. In this paper, we aim to discover symbolic partial differential equations (PDEs) in the form

$$F(\mathbf{x}, u^{(n)}) = 0, \quad (1)$$

where \mathbf{x} denotes the independent variables, $u^{(n)}$ consists of the dependent variable u and all of its up-to- n th order partial derivatives.

While it has long been an exclusive task for human experts to identify governing equations, symbolic regression (SR) has emerged as an increasingly popular approach to automate the discovery.¹ SR constructs expressions from a predefined set of atomic entities, such as variables, constants, and mathematical operators, and fits the expressions to data by numerical optimization. Common methods include sparse regression (Brunton et al., 2016; Champion et al., 2019), genetic programming (Cranmer et al., 2019; 2020; Cranmer, 2023), neural networks (Kamienny et al., 2022), etc.

However, symbolic regression algorithms may fail due to the vastness of the search space or produce more complex, less interpretable equations that overfit the data. A widely adopted remedy to these challenges is to incorporate inductive biases derived from physical laws, such as symmetry and conserved quantities, into equation discovery algorithms. Implementing these physical constraints narrows the space for equations and expedites the search process, and it also rules out physically invalid or unnecessarily complex equations.

¹While some literature uses *symbolic regression* specifically for GP-based methods, we use the term interchangeably with *equation discovery* to refer to all algorithms for learning symbolic equations.

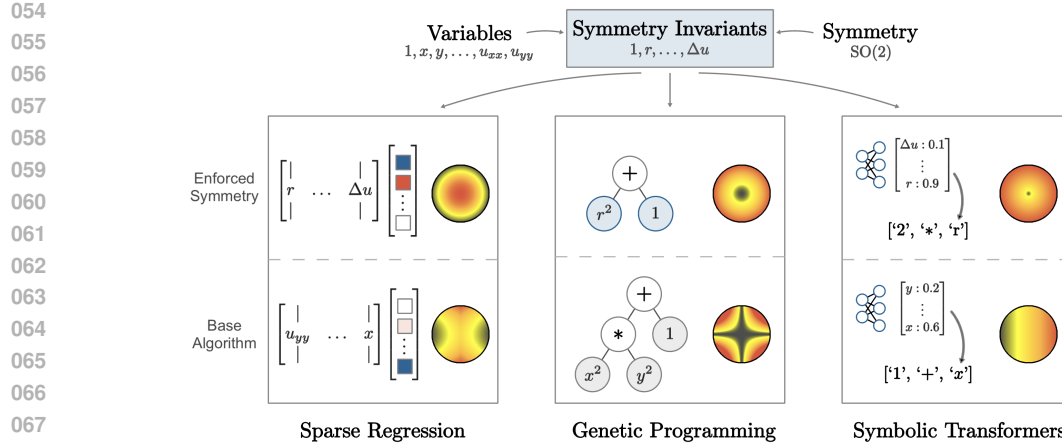


Figure 1: Our framework enforces symmetry in equation discovery by using symmetry invariants. We highlight three discovery algorithms in their original form (bottom row) and when constrained to only use symmetry invariants (top row). The colored circles visualize the predicted functions on a circular domain and demonstrate that using symmetry invariants guarantees a symmetric output.

Among the various physical constraints, symmetry plays a fundamental role in physical systems, governing their invariances under transformations such as rotations, translations, and scaling. Previous research has shown the benefit of incorporating symmetry in equation discovery, such as reducing the dimensionality of the search space and promoting parsimony in the discovered equation (Yang et al., 2024). However, the scopes of existing works exploiting symmetry are limited in terms of the types of equations they can handle, the compatible base algorithms, etc. For example, Udrescu & Tegmark (2020) deals with algebraic equations; Otto et al. (2023) deals with ODE systems; Yang et al. (2024) applies to sparse regression but not other SR algorithms.

In this paper, we propose a general procedure based on *symmetry invariants* to enforce the inductive bias of symmetry with minimal restrictions in the types of equations and SR algorithms. Specifically, we leverage the fact that a differential equation can be written in terms of the invariants of symmetry transformations if it admits a certain symmetry group. Thus, instead of operating on the original variables, our method uses the symmetry invariants as the atomic entities in symbolic regression, as depicted in Figure 1. These invariants encapsulate the essential information while automatically satisfying the symmetry constraints. Consequently, the discovered equations are guaranteed to preserve the specified symmetry. In summary, our main contributions are listed as follows:

- We propose a general framework to enforce symmetry in differential equation discovery based on the theory of differential invariants.
- Our approach can be easily integrated with existing symbolic regression methods, such as sparse regression and genetic programming, and improves their accuracy and efficiency for differential equation discovery.
- We show that our symmetry-based approach is robust in challenging setups in equation discovery, such as noisy data and imperfect symmetry.

Notations. Throughout the paper, subscripts are usually reserved for partial derivatives, e.g. $u_t := \partial u / \partial t$, and $u_{xx} := \partial^2 u / \partial x^2$. Superscripts are used for indexing vector components or list elements. We use Einstein notation, where repeated indices are summed over. Matrices, vectors and scalars are denoted by capital, bold and regular letters, respectively, e.g. W, \mathbf{w}, w . These conventions may admit exceptions for clarity or context. See Table 2 for a full description of notations.

2 BACKGROUND

2.1 PDE SYMMETRY

This section introduces the basic concepts about partial differential equations and their symmetry. For a more thorough understanding of Lie point symmetry of PDEs, we refer the readers to Olver (1993).

108 **Partial Differential Equations.** We consider PDEs in the form $F(\mathbf{x}, u^{(n)}) = 0$, as given in (1). We
 109 restrict ourselves to a single equation and a single dependent variable, unless otherwise stated. We use
 110 $\mathbf{x} \in X \subset \mathbb{R}^p$ to denote all independent variables. For example, $\mathbf{x} = (t, x)$ for a system evolving in
 111 1D space. Note that the bold \mathbf{x} refers to the collection of all independent variables while the regular x
 112 denotes the spatial variable. Then, $u = u(\mathbf{x}) \in U \subset \mathbb{R}$ is the dependent variable; $u^{(n)} = (u, u_x, \dots)$
 113 denotes all up to n th-order partial derivatives of u ; $(\mathbf{x}, u^{(n)}) \in M^{(n)} \subset X \times U^{(n)}$, where $M^{(n)}$ is
 114 the n th order **jet space** of the total space $X \times U$. $M^{(n)}$ and $u^{(n)}$ are also known as the n th-order
 115 **prolongation** of $X \times U$ and u , respectively.

117 **Symmetry of a PDE.** A point symmetry g is a local diffeomorphism on the total space $E = X \times U$:

$$118 \quad g \cdot (\mathbf{x}, u) = (\tilde{\mathbf{x}}(\mathbf{x}, u), \tilde{u}(\mathbf{x}, u)), \quad (2)$$

120 where $\tilde{\mathbf{x}}$ and \tilde{u} are functions of E . The action of g on the function $u(\mathbf{x})$ is induced from (2)
 121 by applying it to the graph of $u : X \rightarrow U$. Specifically, denote the domain of u as $\Omega \subset X$
 122 and its graph as $\Gamma_u = \{(\mathbf{x}, u(\mathbf{x})) : \mathbf{x} \in \Omega\}$. The group element g transforms the graph Γ_u as
 123 $\tilde{\Gamma}_u := g \cdot \Gamma_u = \{(\tilde{\mathbf{x}}, \tilde{u}) = g \cdot (\mathbf{x}, u) : (\mathbf{x}, u) \in \Gamma_u\}$.

124 Since g transforms both independent and dependent variables, $\tilde{\Gamma}_u$ does not necessarily correspond to
 125 the graph of any single-valued function. Nevertheless, by suitably shrinking the domain Ω_X , we can
 126 ensure that the transformations close to the identity transform Γ_u to the graph of another function.
 127 This function with the transformed graph $\tilde{\Gamma}_u$ is then defined to be the transformed function of the
 128 original solution u , i.e. $g \cdot u = \tilde{u}$ s.t. $\tilde{\Gamma}_u = \tilde{\Gamma}_u$. The symmetry of the PDE (1) is then defined:

130 **Definition 2.1.** A symmetry group of $F(\mathbf{x}, u^{(n)}) = 0$ is a local group of transformations G acting
 131 on an open subset of the total space $X \times U$ such that, for any solution u to $F = 0$ and any $g \in G$,
 132 the function $\tilde{u} = (g \cdot u)(\mathbf{x})$ is also a solution of $F = 0$ wherever it is defined.

133 **Infinitesimal Generators.** Often, the symmetry group of a PDE is a continuous Lie group. In
 134 practice, one needs to compute with infinitesimal generators of continuous symmetries, i.e., vector
 135 fields. In more detail, we will write vector fields $\mathbf{v} : E \rightarrow TE$ on $E = X \times U$ as

$$137 \quad \mathbf{v} = \xi^j(\mathbf{x}, u) \frac{\partial}{\partial x^j} + \phi(\mathbf{x}, u) \frac{\partial}{\partial u}. \quad (3)$$

139 Any such vector field generates a one-parameter group of symmetries of the total space $\{\exp(\epsilon \mathbf{v}) : \epsilon \in \mathbb{R}\}$. The symmetries arising from the exponentiation of a vector field moves a point in the total
 140 space along the directions given by the vector field. We will specify symmetries by vector fields in
 141 the following sections. For instance, $\mathbf{v} = x\partial_y - y\partial_x$ represents the rotation in (x, y) -plane; $\mathbf{v} = \partial_t$
 142 corresponds to time translation.

144 To analyze the symmetry of PDEs, we must know how it transforms not only the variables, but also
 145 their derivatives accordingly. The group transformations on derivatives are formalized by **prolonged**
 146 group actions and infinitesimal actions on the n th-order jet space, denoted $g^{(n)}$ and $\mathbf{v}^{(n)}$, respectively.
 147 More details on prolonged group actions are discussed in Appendix B.2, with Figure 4 visualizing a
 148 simple example. To introduce our method, it suffices to note that the prolongation of the vector field
 149 (3) can be described explicitly by ξ^j and ϕ and their derivatives via the *prolongation formula* (9).

151 2.2 SYMBOLIC REGRESSION ALGORITHMS

153 Given the data $\{(x^i, y^i)\} \subset X \times Y$, the objective of symbolic regression is to find a symbolic
 154 expression for the function $y = f(x)$. Although this original formulation is for algebraic equations,
 155 it can be generalized to differential equations like (1). To discover a PDE from the dataset of its
 156 observed solutions on a grid Ω , i.e. $\{(\mathbf{x}, u(\mathbf{x})) : \mathbf{x} \in \Omega\}$, we estimate the partial derivative terms
 157 and add them to the dataset: $\{(\mathbf{x}, u^{(n)}) : \mathbf{x} \in \Omega\}$. One of the variables in the variable set $(\mathbf{x}, u^{(n)})$
 158 is used as the LHS of the equation, i.e. the role of the label y in symbolic regression, while other
 159 variables serve as features. The precise set of derivatives added to symbolic regression and the choice
 160 of the equation LHS requires prior knowledge or speculations about the underlying system.

161 We briefly review two classes of symbolic regression algorithms: sparse regression (SINDy) and
 162 genetic programming (GP). A more detailed discussion of related works is found in Appendix A.

162 **Sparse regression** (Brunton et al., 2016) is specifically designed for discovering differential equations.
 163 It assumes the LHS ℓ of the equation is a fixed term, e.g. $\ell = u_t$, and the RHS of the equation can be
 164 written as a *linear combination* of m predefined functions θ^j with trainable coefficients $\mathbf{w} \in \mathbb{R}^m$, i.e.,
 165

$$166 \ell(\mathbf{x}, u^{(n)}) = w^j \theta^j(\mathbf{x}, u^{(n)}), \theta^j : M^{(n)} \rightarrow \mathbb{R}. \quad (4)$$

167 The equation is found by solving for \mathbf{w} that minimizes the objective $\|\mathbf{L} - \mathbf{R}\|_2^2 + \lambda \|\mathbf{w}\|_0$, where \mathbf{L}
 168 and \mathbf{R} are obtained by evaluating ℓ and $w^j \theta^j$ on all data points and concatenating them into column
 169 vectors, and $\|\mathbf{w}\|_0$ regularizes the number of nonzero terms. This formulation can be easily extended
 170 to q equations and dependent variables ($q > 1$): $\ell^i(\mathbf{x}, \mathbf{u}^{(n)}) = W^{ij} \theta^j(\mathbf{x}, \mathbf{u}^{(n)}), W \in \mathbb{R}^{q \times m}$.
 171

172 One problem with sparse regression is its restrictive assumptions about the form of equations. Many
 173 equations cannot be expressed in the form of (4), e.g. $y = \frac{1}{x+a}$ where a could be any constant. Also,
 174 the success of sparse regression relies on the proper choice of the function library $\{\theta^j\}$. If any term
 175 in the true equation were not included, sparse regression would fail to identify the correct equation.

176 **Genetic programming** (GP) offers an alternative solution for equation discovery (Cranmer, 2023),
 177 which can learn equations in more general forms. It represents each expression as a tree and
 178 instantiates a population of individual expressions. At each iteration, it samples a subset of expressions
 179 and selects one of them that best fits the data; the selected expression is then mutated by a random
 180 mutation, a crossover with another expression, or a constant optimization; the mutated expression
 181 replaces an expression in the population that does not fit the data well. The algorithm repeats this
 182 process to search for different combinations of variables, constants, and operators, and finally returns
 183 the “fittest” expression. GP can be less efficient than sparse regression when the equation can be
 184 expressed in the form (4) due to its larger search space. However, we will show that it is a promising
 185 alternative to discover PDEs of generic forms, and our approach further boosts its efficiency.
 186

187 3 SYMBOLIC REGRESSION WITH SYMMETRY INVARIANTS

188 Symmetry offers a natural inductive bias for the search space of symbolic regression in differential
 189 equations. It reduces the dimensionality of the space and encourages parsimony of the resulting
 190 equations. To enforce symmetry in PDE discovery, we aim to find the maximal set of equations
 191 admitting a *given* symmetry and search in that set with symbolic regression (SR) methods.
 192

193 3.1 DIFFERENTIAL INVARIANTS AND SYMMETRY CONDITIONS

195 To achieve this, our general strategy is to replace the original variable set with a complete set
 196 of *invariant functions* of the given symmetry group. Since we consider PDEs containing partial
 197 derivatives, the invariant functions refer to the *differential invariants* defined as follows.

198 **Definition 3.1** (Def. 2.51, Olver (1993)). Let G be a local group of transformations acting on $X \times U$.
 199 Any $g \in G$ gives a prolonged group action $\text{pr}^{(n)} g$ on the jet space $M^{(n)} \subset X \times U^{(n)}$. An n th
 200 order differential invariant of G is a smooth function $\eta : M^{(n)} \rightarrow \mathbb{R}$, such that for all $g \in G$ and all
 201 $(\mathbf{x}, u^{(n)}) \in M^{(n)}$, $\eta(g^{(n)} \cdot (\mathbf{x}, u^{(n)})) = \eta(\mathbf{x}, u^{(n)})$ whenever $g^{(n)} \cdot (\mathbf{x}, u^{(n)})$ is defined.

203 In other words, differential invariants are functions of all variables and partial derivatives that remain
 204 invariant under prolonged group actions. Equivalently, if G is generated by a set of infinitesimal
 205 generators $\mathcal{B} = \{\mathbf{v}_a\}$, then a function η is a differential invariant of G iff $\mathbf{v}_a^{(n)}(\eta) = 0$ for all $\mathbf{v}_a \in \mathcal{B}$.
 206 The following theorem guarantees that any differential equation admitting a symmetry group can be
 207 expressed solely in terms of the group invariants.

208 **Theorem 3.2** (Prop. 2.56, Olver (1993)). Let G be a local group of transformations acting on $X \times U$.
 209 Let $\{\eta^1(\mathbf{x}, u^{(n)}), \dots, \eta^k(\mathbf{x}, u^{(n)})\}$ be a complete set of functionally independent n th-order differential
 210 invariants of G . An n th-order differential equation (1) admits G as a symmetry group if and only if it
 211 is equivalent to an equation of the form $\tilde{F}(\eta^1, \dots, \eta^k) = 0$.

212 Consequently, SR with a complete set of invariants precisely searches within the space of all symmet-
 213 ric differential equations and automatically excludes equations violating the specified symmetry.

215 Our strategy of using differential invariants applies broadly to various equation discovery algorithms.
 For instance, in sparse regression, we can construct the function library using invariants rather than

raw variables and derivatives. Similarly, in genetic programming, the variable set can be redefined to include only invariant functions. In each case, the key benefit is the same: the search space is restricted to symmetry-respecting equations by construction. The reduced complexity of the equation search also leads to increased accuracy and efficiency.

Next, we describe how to construct a complete set of differential invariants (Section 3.2), and how to incorporate them into specific SR algorithms (Section 3.3).

3.2 CONSTRUCTING A COMPLETE SET OF INVARIANTS

Despite the simplicity of our strategy, we still need a concrete method for computing the invariants. In this subsection, we provide a general guideline to construct a complete set of differential invariants up to a required order given the group action.

By definition of differential invariants, we look for functions $\eta(\mathbf{x}, u^{(n)})$ satisfying $\mathbf{v}^{(n)}(\eta) = 0$ given a prolonged vector field $\mathbf{v}^{(n)}$. This is a first-order linear PDE that can be solved by the method of characteristics. However, in practice, if $E = X \times U \simeq \mathbb{R}^p \times \mathbb{R}$, there are $\binom{p+n-1}{n}$ partial derivatives of the independent variable u of order exactly n . Therefore, as n grows, it quickly becomes impractical to solve directly for n th-order differential invariants. The higher-order differential invariants, if necessary, can be computed recursively from lower-order ones by the following result:

Proposition 3.3. *Let G be a local group of transformations acting on $X \times U \simeq \mathbb{R}^p \times \mathbb{R}$. Let $\eta^1, \eta^2, \dots, \eta^p$ be any p differential invariants of G whose horizontal Jacobian $J = [D_i \eta^j]$ is non-degenerate on an open subset $\Omega \subset M^{(n)}$. If there are a maximal number of independent, strictly n th-order differential invariants $\zeta^1, \dots, \zeta^{q_n}$, $q_n = \binom{p+n-1}{n}$, then the following set contains a complete set of independent, strictly $(n+1)$ th-order differential invariants defined on Ω :*

$$\det(D_i \tilde{\eta}_{(k, k')}^j) / \det(D_i \eta^j), \forall k \in [p], k' \in [q_n], \quad (5)$$

where $i, j \in [p]$ are matrix indices, D_i denotes the total derivative w.r.t i -th independent variable and $\tilde{\eta}_{(k, k')}^j = [\eta^1, \dots, \eta^{k-1}, \zeta^{k'}, \eta^{k+1}, \dots, \eta^p]$.

In practice, we first solve for $\mathbf{v}(\eta) = 0$ to obtain a sufficient number of lower-order invariants as required in Proposition 3.3, and then construct complete sets of invariants of arbitrary orders. Notably, while in theory our framework operates on any complete set of differential invariants, the invariants computed this way may be algebraically complicated and poorly scaled, leading to difficulties in SR optimization. In practice, we start from such a complete set of differential invariants and then deliberately convert them into simpler, physically interpretable invariant functions (such as Laplacians for rotational symmetry) as the feature set for SR. We evaluate invariants on the dataset only where they are well-defined. If necessary, we shrink the domain and filter out data points that cause singularity (e.g., where the denominator of an invariant function vanishes). In Appendix B.4, we provide two examples of different symmetry groups and their differential invariants. Those results will also be used in our experiments.

3.3 IMPLEMENTATION IN SR ALGORITHMS

Our symmetry principle characterizes a subspace of all equations with a given symmetry. Generally, this subspace partially overlaps with the hypothesis spaces of SR algorithms, conceptually visualized in Figure 2. As in Theorem 3.2, PDEs with symmetry can be expressed as *implicit* functions of all differential invariants. However, symbolic regression methods typically learn *explicit* functions mapping features to labels. Some algorithms, such as SINDy, impose even stronger constraints on equation forms. Therefore, adaptation is needed to implement our strategy of using differential invariants in specific symbolic regression algorithms, as detailed below.

General explicit SR We start with general SR methods that learn an *explicit* function $y = f(x)$ without additional assumptions about the form of f , e.g., genetic programming and symbolic transformer. When learning the equation with differential invariants, we do not know which one of them

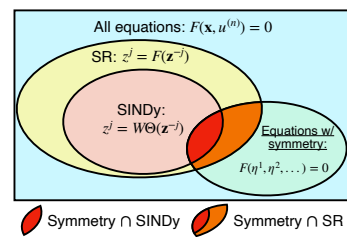


Figure 2: Venn diagram of hypothesis spaces from base SR methods and our symmetry principle.

270 should be used as the LHS of the equation, i.e. the label y in symbolic regression. Thus, we fit an
 271 equation for each invariant as LHS and choose the equation with the lowest data error, as described in
 272 Algorithm 1. We use relative error to select the best equation since the scales of LHS terms differ.
 273
 274

275 Algorithm 1 General explicit SR for differential equations with symmetry invariants

276 **Require:** PDE order n , dataset $\{\mathbf{z}^i = (\mathbf{x}^i, (u^{(n)})^i) \in M^{(n)}\}_{i=1}^{N_D}$, base SR algorithm $\mathcal{S} : (\mathbf{X}, \mathbf{y}) \mapsto$
 277 $y = f(x)$, infinitesimal generators of the symmetry group $\mathcal{B} = \{\mathbf{v}_a\}$.

278 **Ensure:** A PDE admitting the given symmetry group.

279 Compute the symmetry invariants of \mathcal{B} up to n th-order: η^1, \dots, η^K . {Prop. 3.3}

280 Evaluate the invariant functions on the dataset: $\eta^{k,i} = \eta^k(\mathbf{z}^i)$, for $k \in [K], i \in [N_D]$.

281 Initialize a list of candidate equations and their risks: $\mathbf{E} = []$.

282 **for** k in $1 : K$ **do**

283 Use the k th invariant as label and the rest as features: $\mathbf{y} = \eta^{k,:}, \mathbf{X} = \eta^{-k,:}$.

284 Run $\mathcal{S}(\mathbf{X}, \mathbf{y})$ and get a candidate equation $\eta^k = f^k(\eta^{-k})$.

285 Evaluate $\mathcal{L}^k = \|\mathbf{y} - f^k(\mathbf{X})\|_1 / \|\mathbf{y}\|_1$ and set $\mathbf{E}[k] = (f^k, \mathcal{L}^k)$.

286 **end for**

287 Choose the equation in \mathbf{E} with the lowest error: $k = \arg \min_j \mathbf{E}[j][2]$.

288 **return** $\eta^k = f^k(\eta^{-k})$. {Optionally, expand all η^j in terms of original variables \mathbf{z} .}

291 **Sparse regression** SINDy assumes a linear equation form (4). Generally, its function library differs
 292 from the set of differential invariants. Also, SINDy fixes a LHS term, while we do not single out an
 293 invariant as the LHS of the equation when constructing the set of invariants.

294 Assume we are provided the SINDy configuration, i.e. the LHS term ℓ and the function library $\{\theta^j\}$.
 295 To implement sparse regression with symmetry invariants, we assign an invariant η^k that symbolically
 296 depends on ℓ , i.e. $\partial \eta^k / \partial \ell \neq 0$, as the LHS for the equation in terms of symmetry invariants. The
 297 remaining invariants are included on the RHS, where they serve as inputs of the original SINDy
 298 library functions. In other words, the equation form is $\eta^k = \tilde{w}^j \theta^j(\eta^{-k})$. Similar to Algorithm 1, we
 299 can expand all η variables to obtain the equation in original jet variables.
 300

301 The above approach optimizes an unconstrained coefficient vector \tilde{w} for functions of symmetry
 302 invariants. Alternatively, we can use the original SINDy equation form (4) and implement the
 303 symmetry constraint as a constraint on the coefficient w , as demonstrated in the following theorem.
 304 Here, we generalize the setup to multiple dependent variables and equations.

305 **Proposition 3.4.** Let $\ell(\mathbf{x}, \mathbf{u}^{(n)}) = W\theta(\mathbf{x}, \mathbf{u}^{(n)})$ be a system of q differential equations admitting a
 306 symmetry group G , where $\mathbf{x} \in \mathbb{R}^p$, $\mathbf{u} \in \mathbb{R}^q$, $\theta \in \mathbb{R}^m$. Assume there exist some n th-order invariants
 307 of G , $\eta_0^{1:q}$ and $\eta^{1:K}$, s.t. (1) the system of equations can be expressed as $\eta_0 = W'\theta'(\eta)$, where
 308 $\eta_0 = [\eta_0^{1:q}]$ and $\eta = [\eta^{1:K}]$, and (2) $\eta_0^i = T^{ijk} \theta^k \ell^j$ and $(\theta')^i = S^{ij} \theta^j$, for some functions $\theta'(\eta)$
 309 and constant tensors W' , T and S . Then, the space of all possible W is a linear subspace of $\mathbb{R}^{q \times m}$.

311 Intuitively, the conditions above state that the equations can be expressed as a linear combination of
 312 invariant terms, similar to the form in (4) w.r.t original jet variables. Also, every invariant term in
 313 η_0 and $\theta'(\eta)$ is already encoded in the original library θ . In practice, we need to choose a suitable
 314 set of invariants according to the SINDy configuration to meet these conditions. For example, when
 315 θ contains all monomials on $M^{(n)}$ up to degree d , any set of invariants where each invariant is
 316 a polynomial on $M^{(n)}$ up to degree d satisfies these conditions. The proof of Proposition 3.4 is
 317 provided in Appendix B, where we explicitly identify the basis of the linear subspace for W .

318 Proposition 3.4 allows us to keep track of the original SINDy parameters W during optimization.
 319 This enables straightforward integration of symmetry constraints to variants of SINDy, e.g. Weak
 320 SINDy (Messenger & Bortz, 2021a;b) for noisy data. For example, if the constrained subspace has a
 321 basis $Q \in \mathbb{R}^{r \times q \times m}$, where r is the subspace dimension, we write $W^{jk} = Q^{ijk} \beta^i$. While we directly
 322 optimize β , we can still easily compute the objective of Weak SINDy which explicitly depends on
 323 W . In comparison, if we use the raw invariant terms for regression, e.g. the equations take the form
 $\eta_0 = W'\theta'(\eta)$, it is challenging to formulate the objective of Weak SINDy w.r.t W' .

324 3.4 CONSTRAINT RELAXATION FOR SYSTEMS WITH IMPERFECT SYMMETRY
325

326 Our approach discovers PDEs assuming perfect symmetry. However, it is common in reality that
327 a system shows imperfect symmetry due to external forces, boundary conditions, etc. (Wang et al.,
328 2022). In such cases, the previous method cannot identify any symmetry-breaking factors.

329 To address this, we propose to relax the symmetry constraints by allowing symmetry-breaking terms
330 to appear in the equation, but at a higher “cost”. We implement this idea in sparse regression, where
331 the equation has a linear structure $\ell = W\theta$. We adopt the technique from Residual Pathway Prior
332 (RPP) (Finzi et al., 2021), which is originally developed for equivariant linear layers in neural nets.
333 Specifically, let Q be the basis of the parameter subspace that preserves symmetry and P be the
334 orthogonal complement of Q . Instead of parameterizing W in this subspace, we define $W = A + B$
335 where $A^{jk} = Q^{ijk}\beta^i$ and $B^{jk} = P^{ijk}\gamma^i$ and place a stronger regularization on γ than on β . While the
336 model still favors equations in the symmetry subspace spanned by Q , symmetry-breaking components
337 in P can appear if it fits the data well.

338 More implementation details related to Section 3.3 and 3.4 can be found in Appendix C.
339

340 4 EXPERIMENTS
341342 4.1 DATASETS AND THEIR SYMMETRIES
343

344 We consider the following PDE systems, which cover different challenges in PDE discovery, such
345 as high-order derivatives, generic equation form, multiple dependent variables and equations, noisy
346 dataset, and imperfect symmetry. The datasets are generated by simulating the ground truth equation
347 from specified initial conditions, with detailed procedures described in Appendix E.1.

348 **Boussinesq Equation.** Consider the Boussinesq equation describing the unidirectional propagation
349 of a solitary wave in shallow water (Newell, 1985):
350

$$u_{tt} + uu_{xx} + u_x^2 + u_{xxxx} = 0 \quad (6)$$

351 This equation has a scaling symmetry $\mathbf{v}_1 = 2t\partial_t + x\partial_x - 2u\partial_u$ and the translation symmetries in
352 space and time. The differential invariants are given by $\eta_{(\alpha,\beta)} = u_{x^{(\alpha)}t^{(\beta)}}u_x^{-(2+\alpha+2\beta)/3}$ where α
353 and β are the orders of partial derivatives in x and t , respectively. To discover the 4th-order equation,
354 we compute all $\eta_{(\alpha,\beta)}$ for $0 \leq \alpha + \beta \leq 4$, except for $\eta_{(1,0)} = 1$ which is a constant.
355

356 **Darcy Flow.** The following PDE describes the steady state of a 2D Darcy flow (Takamoto et al.,
357 2022) with spatially varying viscosity $a(x, y) = e^{-4(x^2+y^2)}$ and a constant force term $f(x) = 1$:
358

$$-\nabla(e^{-4(x^2+y^2)}\nabla u) = 1 \quad (7)$$

360 This equation admits an $SO(2)$ rotation symmetry $\mathbf{v} = y\partial_x - x\partial_y$. A detailed calculation of
361 the differential invariants of this group can be found in Example B.5. In our experiment, we use
362 the following complete set of 2nd-order invariants: $\{\frac{1}{2}(x^2 + y^2), u, xu_y - yu_x, xu_x + yu_y, u_{xx} +$
363 $u_{yy}, u_{xx}^2 + 2u_{xy}^2 + u_{yy}^2, x^2u_{xx} + y^2u_{yy} + 2xyu_{xy}\}$.
364

365 **Reaction-Diffusion.** We consider the following system of PDEs from Champion et al. (2019):
366

$$\begin{aligned} u_t &= d_1 \nabla^2 u + (1 - u^2 - v^2)u + (u^2 + v^2)v \\ v_t &= d_2 \nabla^2 v - (u^2 + v^2)u + (1 - u^2 - v^2)v \end{aligned} \quad (8)$$

367 In the default setup, we use $d_1 = d_2 = 0.1$. The system then exhibits rotational symmetry in the
368 phase space: $\mathbf{v} = u\partial_v - v\partial_u$. The ordinary invariants (functions of variables, not derivatives) are
369 $\{t, x, y, u^2 + v^2\}$. The higher-order invariants are $\{\mathbf{u} \cdot \mathbf{u}_\mu, \mathbf{u}^\perp \cdot \mathbf{u}_\mu\}$, where $\mathbf{u} = (u, v)^T$ and μ is
370 any multi-index of t, x and y .
371

372 We also consider the following cases where the rotation symmetry is broken due to different factors:
373

- 374 • **Unequal diffusivities** We use different diffusion coefficients for the two components: $d_1 = 0.1$, $d_2 = 0.1 + \epsilon$. This can happen, for example, when two chemical species described by the
375 equation diffuse at different rates due to molecular size, charge, or solvent interactions.
376
- 377 • **External forcing** The ground truth equation (8) is modified by adding $-\epsilon v$ to the RHS of u_t and $-\epsilon u$ to the RHS of v_t . This can reflect a weak parametric forcing on the system.
378

378
379

4.2 METHODS AND EVALUATION CRITERIA

380
381
382
383
384

We consider three classes of algorithms for equation discovery: sparse regression (PySINDy, de Silva et al. (2020); Kaptanoglu et al. (2022)), genetic programming (PySR, Cranmer (2023)), and a pretrained symbolic transformer (E2E, Kamienny et al. (2022)). For each class, we compare the original algorithm using the regular jet space variables (i.e. $(\mathbf{x}, u^{(n)})$) and our method using symmetry invariants. Our method will be referenced as SI (Symmetry Invariants) in the results.

385
386
387
388
389
390
391
392
393
394
395
396
397

To evaluate an equation discovery algorithm, we run it 100 times with randomly sampled data subsets and randomly initialized models if applicable. We record its *success probability* (SP) of discovering the correct equation. Specifically, we expand the ground truth equation into $\sum_i c^i f^i(\mathbf{z}) = 0$, where c^i are nonzero coefficients, \mathbf{z} denotes the variables involved in the algorithm, i.e., original jet variables $(\mathbf{x}, u^{(n)})$ for baselines and symmetry invariants for our method, and f^i are functions of \mathbf{z} . Also, the discovered equation is expanded as $\sum_i \hat{c}^i \hat{f}^i(\mathbf{z}) = 0$, where $\hat{c}^i \neq 0$. The discovered equation is considered correct if all the terms with nonzero coefficients match the ground truth, i.e., $\{f^i\} = \{\hat{f}^i\}$. We also report the *prediction error* (PE), which measures how well the discovered equation fits the data. For evolution equations with time derivatives on the LHS, we simulate each discovered equation from an initial condition and measure its difference from the ground truth solution at a specific timestep in terms of root mean square error (RMSE). Otherwise, we just report the RMSE of the discovered equation evaluated on all test data points.

398
399

4.3 RESULTS ON CLEAN DATA WITH PERFECT SYMMETRY

400
401
402
403
404
405

Table 1: Equation discovery results on clean data. \mathcal{C} , standing for *complexity*, refers to the effective parameter space dimension in sparse regression and the number of variables in GP/Transformer. SP and PE stands for *success probability* and *prediction error*, as explained in Section 4.2. The entries “-” suggest that the method does not apply to the specific PDE system, or the result is not meaningful. The arrows \uparrow / \downarrow mean higher/lower metrics are better.

Method		Boussinesq (6)			Darcy flow (7)			Reaction-diffusion (8)		
		$\mathcal{C} \downarrow$	SP \uparrow	PE \downarrow	$\mathcal{C} \downarrow$	SP \uparrow	PE \downarrow	$\mathcal{C} \downarrow$	SP \uparrow	PE \downarrow
Sparse Regression	PySINDy	15	0.00	0.373	-	-	-	38	0.53	0.021
	SI	13	1.00	0.098	-	-	-	28	0.54	0.008
Genetic Programming	PySR	17	0.90	0.098	8	0.00	0.114	17	0.00	-
	SI	14	1.00	0.098	7	0.79	0.051	16	0.81	0.023
Transformer	E2E	10	0.53	0.132	8	0.00	-	17	0.00	-
	SI	7	0.85	0.104	7	0.00	-	16	0.00	-

414

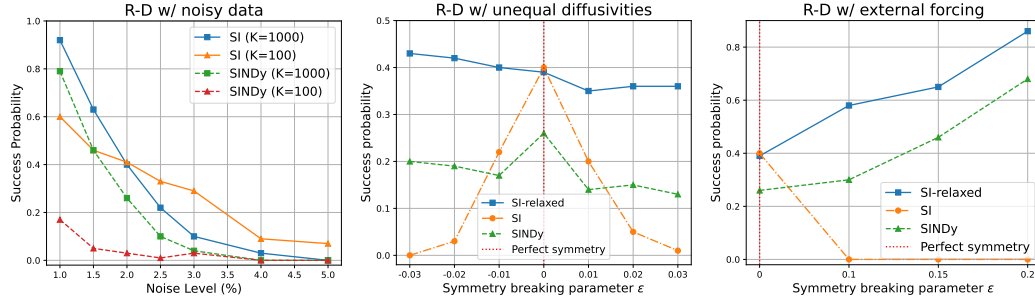
Table 1 summarizes the performance of all methods on the three PDE systems. For prediction errors (PE), we report the median, instead of the average, of 100 runs for each algorithm, because some incorrectly discovered equations yield tremendous prediction errors. Comparisons are made within each class of methods. Generally, using symmetry invariants reduces the complexity of equation discovery and improves the chance of finding the correct equations compared to the baselines.

420
421
422
423
424
425

Specifically, in sparse regression, our method using symmetry invariants is only slightly better than PySINDy in the reaction-diffusion system, but constantly succeeds in the Boussinesq equation where PySINDy fails. The failure of PySINDy is because the u_x^2 term in (6) is not supported by its function library, showing that SINDy’s success relies heavily on the choice of function library. On the other hand, by enforcing the equation to be expressed in invariants, our method automatically identifies the proper function library. Appendix D.2 provides results for other variants of sparse regression.

426
427
428
429
430
431

For GP-based methods, Table 1 displays the results with a fixed number of GP iterations for each dataset. We also include results with different numbers of iterations in Appendix D.3. Generally, GP with invariants can identify the correct equation with fewer iterations and is considered more efficient. On the other hand, the pretrained symbolic transformer fails on two of the three datasets. We conjecture this is because the data distribution from PDE solutions greatly differs from its pretraining dataset. However, the symbolic transformer can discover the Boussinesq equation correctly, where using symmetry invariants leads to much higher success probability.

432 4.4 RESULTS ON NOISY DATA AND IMPERFECT SYMMETRY
433434 We test the robustness of our method under two challenging scenarios: (1) noise in observed data,
435 and (2) PDE with imperfect symmetry.436
437 Figure 3: Success probabilities of sparse regression methods on the reaction-diffusion system with
438 noisy data (left), unequal diffusivities (center) and external forcing (right). Under noisy data, our
439 method (SI) consistently outperforms SINDy under the same number of test functions. For systems
440 with imperfect symmetry, strictly enforcing symmetry (SI) hurts performance, but a relaxed symmetry
441 constraint (SI-relaxed, introduced in Section 3.4) is still better than no inductive bias (SINDy).
442443 In the first experiment, we add different levels of white noise to the simulated solution of the reaction-
444 diffusion system. Since the derivatives estimated by finite difference is inaccurate with the noisy
445 solution, we use the weak formulation of SINDy (Messenger & Bortz, 2021a), which does not require
446 derivative estimation. The success probabilities of our method (SI) and SINDy are shown in Figure 3
447 (left), where K is the number of test functions in weak SINDy. With the same K , our method
448 consistently achieves higher success probability at different noise levels. Notably, when the noise
449 level is high, our symmetry-constrained model performs better with fewer test functions ($K = 100$).
450 We comment that choosing test functions and related hyperparameters is known to be a challenging
451 problem (Tran & Bortz, 2025), and we leave further investigation of this phenomenon to future work.
452453 In the second experiment, we simulate the two variants of (8) (unequal diffusivities and external
454 forcing) with different values for the symmetry-breaking parameter ϵ and add 2% noise to the
455 numerical solutions. We compare three models: (1) our model with strictly enforced symmetry (SI),
456 (2) our model with relaxed symmetry (SI-relaxed) introduced in Section 3.4, and (3) weak SINDy as
457 the baseline. The results for the two systems with symmetry breaking are shown in Figure 3 (center
& right). As expected, SI has a much lower success probability when the symmetry-breaking factor
458 becomes significant. Meanwhile, SI-relaxed remains highly competitive. It also has a clear advantage
459 over baseline SINDy, showing that even if the inductive bias of symmetry is slightly inaccurate, our
460 model with relaxed constraints is still better than a model without any knowledge of symmetry.
461462 More comprehensive results, e.g. variant sparse regression models, comparison with D-CIPHER
463 (Kacprzyk et al., 2023) baseline, discovered equation samples, are provided in Appendix D.
464

465 5 DISCUSSION

466 We propose to enforce symmetry in symbolic regression algorithms for discovering PDEs by using
467 differential invariants of the symmetry group as the variable set. We implement this general strategy in
468 different classes of algorithms and observe improved accuracy, efficiency and robustness of equation
469 discovery, especially in challenging scenarios such as noisy data and imperfect symmetry.
470471 It should be noted that our method assumes the symmetry group is already given. This assumption
472 aligns with common practice: physicists often begin by hypothesizing the symmetries of a system and
473 seek governing equations allowed by those symmetries. However, our current framework cannot be
474 applied if symmetry is unknown, and will produce incorrect results with misspecified symmetry. This
475 can be potentially addressed by incorporating automated symmetry discovery methods for differential
476 equations (Yang et al., 2024; Ko et al., 2024), which we leave for future work.
477478 Another caveat of our method is the calculation of differential invariants. While solving for $\mathbf{v}^{(n)}(\eta) =$
479 0 and applying the formula (5) is easy with any symbolic computation package, the resulting
480 differential invariants may be complicated and require ad-hoc adjustment for better interpretability
481

486 and compatibility with specific algorithm implementations (e.g. conditions in Proposition 3.4).
 487 Fortunately, this only requires a one-time effort. Once we have derived the invariants for a symmetry
 488 group, the results can be reused for any equation admitting the same symmetry.
 489

490 **ETHICS STATEMENT**
 491

492 All authors of this paper have read and agreed to adhere to the ICLR Code of Ethics. We believe that
 493 this paper does not pose any significant ethical concerns that need to be highlighted here.
 494

495 **REPRODUCIBILITY STATEMENT**
 496

497 To ensure the reproducibility of the experiments in this paper, we have provided detailed experimental
 498 instructions for both data generation and symbolic regression methods in Appendix E. Also, we have
 499 provided the codebase to run the experiments in the supplementary material of this submission.
 500

501 **REFERENCES**
 502

503 Tara Akhound-Sadegh, Laurence Perreault-Levasseur, Johannes Brandstetter, Max Welling, and
 504 Siamak Ravanbakhsh. Lie point symmetry and physics informed networks. *arXiv preprint*
 505 *arXiv:2311.04293*, 2023.

506 Joseph Bakarji, Jared Callaham, Steven L. Brunton, and J. Nathan Kutz. Dimensionally consistent
 507 learning with buckingham pi. *Nature Computational Science*, 2:834–844, 12 2022. ISSN 2662-
 508 8457. doi: 10.1038/s43588-022-00355-5.

509 Luca Biggio, Tommaso Bendinelli, Alexander Neitz, Aurelien Lucchi, and Giambattista Parascandolo.
 510 Neural symbolic regression that scales. In Marina Meila and Tong Zhang (eds.), *Proceedings of*
 511 *the 38th International Conference on Machine Learning*, volume 139 of *Proceedings of Machine*
 512 *Learning Research*, pp. 936–945. PMLR, 18–24 Jul 2021.

513 Johannes Brandstetter, Max Welling, and Daniel E Worrall. Lie point symmetry data augmentation
 514 for neural pde solvers. In *International Conference on Machine Learning*, pp. 2241–2256. PMLR,
 515 2022.

516 Steven L. Brunton, Joshua L. Proctor, and J. Nathan Kutz. Discovering governing equations from data
 517 by sparse identification of nonlinear dynamical systems. *Proceedings of the National Academy of*
 518 *Sciences*, 113(15):3932–3937, 2016. doi: 10.1073/pnas.1517384113.

519 Kathleen Champion, Bethany Lusch, J. Nathan Kutz, and Steven L. Brunton. Data-driven discovery
 520 of coordinates and governing equations. *Proceedings of the National Academy of Sciences*, 116
 521 (45):22445–22451, 2019. doi: 10.1073/pnas.1906995116.

522 Miles Cranmer. Interpretable machine learning for science with pysr and symbolicregression.jl, 2023.

523 Miles Cranmer, Alvaro Sanchez Gonzalez, Peter Battaglia, Rui Xu, Kyle Cranmer, David Spergel,
 524 and Shirley Ho. Discovering symbolic models from deep learning with inductive biases. In
 525 H. Larochelle, M. Ranzato, R. Hadsell, M.F. Balcan, and H. Lin (eds.), *Advances in Neural*
 526 *Information Processing Systems*, volume 33, pp. 17429–17442. Curran Associates, Inc., 2020.

527 Miles D. Cranmer, Rui Xu, Peter Battaglia, and Shirley Ho. Learning symbolic physics with graph
 528 networks, 2019.

529 David Dalton, Dirk Husmeier, and Hao Gao. Physics and lie symmetry informed gaussian processes.
 530 In *Forty-first International Conference on Machine Learning*, 2024.

531 Brian de Silva, Kathleen Champion, Markus Quade, Jean-Christophe Loiseau, J. Kutz, and Steven
 532 Brunton. Pysindy: A python package for the sparse identification of nonlinear dynamical systems
 533 from data. *Journal of Open Source Software*, 5(49):2104, 2020. doi: 10.21105/joss.02104. URL
 534 <https://doi.org/10.21105/joss.02104>.

535 Renáta Dubčáková. Eureqa: software review, 2011.

540 Marc Finzi, Gregory Benton, and Andrew G Wilson. Residual pathway priors for soft equivariance
 541 constraints. In M. Ranzato, A. Beygelzimer, Y. Dauphin, P.S. Liang, and J. Wortman Vaughan
 542 (eds.), *Advances in Neural Information Processing Systems*, volume 34, pp. 30037–30049. Cur-
 543 ran Associates, Inc., 2021. URL https://proceedings.neurips.cc/paper_files/paper/2021/file/fc394e9935fdb62c8aecd372464e1965-Paper.pdf.

544 Sébastien Gaucel, Maarten Keijzer, Evelyne Lutton, and Alberto Tonda. Learning dynamical systems
 545 using standard symbolic regression. In Miguel Nicolau, Krzysztof Krawiec, Malcolm I. Heywood,
 546 Mauro Castelli, Pablo García-Sánchez, Juan J. Merelo, Victor M. Rivas Santos, and Kevin Sim
 547 (eds.), *Genetic Programming*, pp. 25–36, Berlin, Heidelberg, 2014. Springer Berlin Heidelberg.

548 549

550 Arya Grayeli, Atharva Sehgal, Omar Costilla Reyes, Miles Cranmer, and Swarat Chaudhuri. Symbolic
 551 regression with a learned concept library. *Advances in Neural Information Processing Systems*, 37:
 552 44678–44709, 2024.

553 Arthur Grundner, Tom Beucler, Pierre Gentine, and Veronika Eyring. Data-driven equation discovery
 554 of a cloud cover parameterization. *arXiv preprint arXiv:2304.08063*, 2023.

555

556 Daniel R Gurevich, Matthew R Golden, Patrick AK Reinbold, and Roman O Grigoriev. Learning
 557 fluid physics from highly turbulent data using sparse physics-informed discovery of empirical
 558 relations (spider). *Journal of Fluid Mechanics*, 996:A25, 2024.

559

560 Samuel Holt, Zhaozhi Qian, and Mihaela van der Schaar. Deep generative symbolic regression. *arXiv
 561 preprint arXiv:2401.00282*, 2023.

562

563 Krzysztof Kacprzyk, Zhaozhi Qian, and Mihaela van der Schaar. D-cipher: discovery of closed-
 564 form partial differential equations. *Advances in Neural Information Processing Systems*, 36:
 27609–27644, 2023.

565

566 Kadierdan Kaheman, J Nathan Kutz, and Steven L Brunton. Sindy-pi: a robust algorithm for parallel
 567 implicit sparse identification of nonlinear dynamics. *Proceedings of the Royal Society A*, 476
 568 (2242):20200279, 2020.

569

570 Pierre-Alexandre Kamienny, Stéphane d’Ascoli, Guillaume Lample, and François Charton. End-to-
 571 end symbolic regression with transformers. *Advances in Neural Information Processing Systems*,
 35:10269–10281, 2022.

572

573 Alan A. Kaptanoglu, Brian M. de Silva, Urban Fasel, Kadierdan Kaheman, Andy J. Goldschmidt,
 574 Jared Callaham, Charles B. Delahunt, Zachary G. Nicolaou, Kathleen Champion, Jean-Christophe
 575 Loiseau, J. Nathan Kutz, and Steven L. Brunton. Pysindy: A comprehensive python package for
 576 robust sparse system identification. *Journal of Open Source Software*, 7(69):3994, 2022. doi:
 577 10.21105/joss.03994. URL <https://doi.org/10.21105/joss.03994>.

578

579 Gyeonghoon Ko, Hyunsu Kim, and Juho Lee. Learning infinitesimal generators of continuous
 580 symmetries from data. *arXiv preprint arXiv:2410.21853*, 2024.

581

582 Kookjin Lee, Nathaniel Trask, and Panos Stinis. Structure-preserving sparse identification of nonlinear
 583 dynamics for data-driven modeling. In Bin Dong, Qianxiao Li, Lei Wang, and Zhi-Qin John Xu
 584 (eds.), *Proceedings of Mathematical and Scientific Machine Learning*, volume 190 of *Proceedings
 585 of Machine Learning Research*, pp. 65–80. PMLR, 15–17 Aug 2022.

586

587 Georg Martius and Christoph H Lampert. Extrapolation and learning equations. *arXiv preprint
 588 arXiv:1610.02995*, 2016.

589

590 Matteo Merler, Katsiaryna Haitsiukevich, Nicola Dainese, and Pekka Marttinen. In-context sym-
 591 bolic regression: Leveraging large language models for function discovery. *arXiv preprint
 592 arXiv:2404.19094*, 2024.

593

594 Daniel A Messenger and David M Bortz. Weak sindy for partial differential equations. *Journal of
 595 Computational Physics*, 443:110525, 2021a.

596

597 Daniel A Messenger and David M Bortz. Weak sindy: Galerkin-based data-driven model selection.
 598 *Multiscale Modeling & Simulation*, 19(3):1474–1497, 2021b.

594 Daniel A Messenger, Joshua W Burby, and David M Bortz. Coarse-graining hamiltonian systems
 595 using wsindy. *Scientific Reports*, 14(1):14457, 2024.
 596

597 Grégoire Mialon, Quentin Garrido, Hannah Lawrence, Danyal Rehman, Yann LeCun, and Bobak
 598 Kiani. Self-supervised learning with lie symmetries for partial differential equations. *Advances in
 599 Neural Information Processing Systems*, 36:28973–29004, 2023.

600 Alan C Newell. *Solitons in mathematics and physics*. SIAM, 1985.
 601

602 Peter J Olver. *Applications of Lie groups to differential equations*, volume 107. Springer Science &
 603 Business Media, 1993.

604 Peter J Olver. *Equivalence, invariants and symmetry*. Cambridge University Press, 1995.
 605

606 Samuel E. Otto, Nicholas Zolman, J. Nathan Kutz, and Steven L. Brunton. A unified framework to
 607 enforce, discover, and promote symmetry in machine learning, 2023.
 608

609 Brenden K Petersen, Mikel Landajuela, T Nathan Mundhenk, Claudio P Santiago, Soo K Kim, and
 610 Joanne T Kim. Deep symbolic regression: Recovering mathematical expressions from data via
 611 risk-seeking policy gradients. *arXiv preprint arXiv:1912.04871*, 2019.

612 Zhaozhi Qian, Krzysztof Kacprzyk, and Mihaela van der Schaar. D-code: Discovering closed-form
 613 odes from observed trajectories. In *International Conference on Learning Representations*, 2022.
 614

615 Chengping Rao, Pu Ren, Yang Liu, and Hao Sun. Discovering nonlinear pdes from scarce data with
 616 physics-encoded learning. *arXiv preprint arXiv:2201.12354*, 2022.

617 Samuel H Rudy, Steven L Brunton, Joshua L Proctor, and J Nathan Kutz. Data-driven discovery of
 618 partial differential equations. *Science advances*, 3(4):e1602614, 2017.
 619

620 Subham Sahoo, Christoph Lampert, and Georg Martius. Learning equations for extrapolation and
 621 control. In *International Conference on Machine Learning*, pp. 4442–4450. PMLR, 2018.

622 Michael Schmidt and Hod Lipson. Distilling free-form natural laws from experimental data. *science*,
 623 324(5923):81–85, 2009.
 624

625 Parshin Shojaee, Kazem Meidani, Shashank Gupta, Amir Barati Farimani, and Chandan K Reddy.
 626 Llm-sr: Scientific equation discovery via programming with large language models. *arXiv preprint
 627 arXiv:2404.18400*, 2024.

628 Parshin Shojaee, Ngoc-Hieu Nguyen, Kazem Meidani, Amir Barati Farimani, Khoa D Doan, and
 629 Chandan K Reddy. Llm-srbench: A new benchmark for scientific equation discovery with large
 630 language models. *arXiv preprint arXiv:2504.10415*, 2025.
 631

632 Makoto Takamoto, Timothy Praditia, Raphael Leiteritz, Daniel MacKinlay, Francesco Alesiani, Dirk
 633 Pflüger, and Mathias Niepert. Pdebench: An extensive benchmark for scientific machine learning.
 634 *Advances in Neural Information Processing Systems*, 35:1596–1611, 2022.

635 April Tran and David Bortz. Weak form scientific machine learning: Test function construction for
 636 system identification. *arXiv preprint arXiv:2507.03206*, 2025.
 637

638 Silviu-Marian Udrescu and Max Tegmark. Ai feynman: A physics-inspired method for symbolic
 639 regression. *Science Advances*, 6(16):eaay2631, 2020.
 640

641 Silviu-Marian Udrescu, Andrew Tan, Jiahai Feng, Orisvaldo Neto, Tailin Wu, and Max Tegmark. Ai
 642 feynman 2.0: Pareto-optimal symbolic regression exploiting graph modularity. *Advances in Neural
 643 Information Processing Systems*, 33:4860–4871, 2020.

644 Rui Wang, Robin Walters, and Rose Yu. Incorporating symmetry into deep dynamics models for
 645 improved generalization. In *International Conference on Learning Representations*, 2021.
 646

647 Rui Wang, Robin Walters, and Rose Yu. Approximately equivariant networks for imperfectly
 648 symmetric dynamics. In *International Conference on Machine Learning*. PMLR, 2022.

648 Yiqun Wang, Nicholas Wagner, and James M Rondinelli. Symbolic regression in materials science.
649 *MRS Communications*, 9(3):793–805, 2019.
650

651 Xiaoyu Xie, Arash Samaei, Jiachen Guo, Wing Kam Liu, and Zhengtao Gan. Data-driven discovery
652 of dimensionless numbers and governing laws from scarce measurements. *Nature Communications*,
653 13(1):7562, 2022. doi: 10.1038/s41467-022-35084-w.

654 Jianke Yang, Wang Rao, Nima Dehmamy, Robin Walters, and Rose Yu. Symmetry-informed
655 governing equation discovery. In *Advances in Neural Information Processing Systems (NeurIPS)*,
656 2024.

657 Zhi-Yong Zhang, Hui Zhang, Li-Sheng Zhang, and Lei-Lei Guo. Enforcing continuous symmetries
658 in physics-informed neural network for solving forward and inverse problems of partial differential
659 equations. *Journal of Computational Physics*, 492:112415, 2023.
660

661
662
663
664
665
666
667
668
669
670
671
672
673
674
675
676
677
678
679
680
681
682
683
684
685
686
687
688
689
690
691
692
693
694
695
696
697
698
699
700
701

702 A RELATED WORKS

704 **Symbolic Regression.** Given the dataset $\{(x^i, y^i)\} \subset X \times Y$, symbolic regression (SR) aims to
 705 model the function $y = f(x)$ by a symbolic equation. A popular method for symbolic regression
 706 is genetic programming (GP) (Schmidt & Lipson, 2009; Gaucel et al., 2014), which leverages
 707 evolutionary algorithms to explore the space of possible equations and has demonstrated success in
 708 uncovering governing laws in various scientific domains such as material science (Wang et al., 2019),
 709 climate modeling (Grundner et al., 2023), cosmology (Cranmer et al., 2020), etc. Various software
 710 have been developed for GP-based symbolic regression, e.g. Eureqa (Dubčáková, 2011) and PySR
 711 (Cranmer, 2023).

712 Another class of methods is sparse regression (Brunton et al., 2016), which assumes the function to
 713 be discovered can be written as a linear combination of predefined candidate functions and solves
 714 for the coefficient matrix. It has also been extended to discover more general equations, such as
 715 equations in latent variables (Champion et al., 2019) and PDEs (Rudy et al., 2017).

716 Neural networks have also shown their potential in symbolic regression. Martius & Lampert (2016);
 717 Sahoo et al. (2018) represents a few earliest attempts, where they replace the activation functions
 718 in fully connected networks with math operators and functions, so the network itself translates to
 719 a symbolic formula. Other works represent mathematical expressions as sequences of tokens and
 720 train neural networks to predict the sequence given a dataset of input-output pairs. For example,
 721 Petersen et al. (2019) trains an RNN with policy gradients to minimize the regression error. Biggio
 722 et al. (2021), Kamienny et al. (2022) and Holt et al. (2023) pre-train an encoder-decoder network
 723 over a large amount of procedurally generated equations and query the pretrained model on a new
 724 dataset of input-output pairs at test time.

725 The aforementioned symbolic regression methods can be improved by incorporating specific domain
 726 knowledge. For example, AI Feynman (Udrescu & Tegmark, 2020; Udrescu et al., 2020) uses
 727 properties like separability and compositionality to simplify the data. Cranmer et al. (2020) specifies
 728 the overall skeleton of the equation and fits each part with genetic programming independently. The
 729 goal of this paper falls into this category – to use the knowledge of symmetry to reduce the search
 730 space of symbolic regression and improve its accuracy and efficiency.

731 Recently, Large Language Models (LLMs) have emerged as an alternative for SR, using pre-trained
 732 scientific priors to propose sequential hypothesis (Merler et al., 2024) or to guide genetic program-
 733 ming (Shojaee et al., 2024), balancing the efficiency of domain knowledge with the robustness of
 734 evolutionary search. However, current LLM-based methods often rely on memorizing known equa-
 735 tions rather than facilitating genuine discovery, and their guidance lacks interpretability, specifically,
 736 the reasoning behind their suggestions, evidenced by a recent benchmark specially designed for
 737 LLM-SR (Shojaee et al., 2025). A recent effort sought to improve interpretability by binding symbolic
 738 evolution with natural language explanations (Grayeli et al., 2024). However, this method relies on
 739 frontier LLMs to conduct the evolution of the natural language components, rendering the process
 740 itself opaque. These limitations highlight the need for approaches that enhance the controllability and
 741 explainability of the prior knowledge injected, ensuring more transparent and trustworthy discovery.

742 **Discovering Differential Equations.** While it remains in the scope of symbolic regression, the
 743 discovery of differential equations poses additional challenges because the derivatives are not directly
 744 observed from data. Building upon the aforementioned SINDy sparse regression (Brunton et al.,
 745 2016), Messenger & Bortz (2021a;b) formulates an alternative optimization problem based on the
 746 variational form of differential equations and bypasses the need for derivative estimation. A similar
 747 variational approach is also applied to genetic programming (Qian et al., 2022). Various other
 748 improvements have been made, including refined training procedure (Rao et al., 2022), relaxed
 749 assumptions about the form of the equation (Kaheman et al., 2020), and the incorporation of physical
 750 priors (Xie et al., 2022; Bakarji et al., 2022; Lee et al., 2022; Messenger et al., 2024).

751 **PDE Symmetry in Machine Learning.** Symmetry is an important inductive bias in machine
 752 learning. In the context of learning differential equation systems, many works encourage symmetry
 753 in their models through data augmentation (Brandstetter et al., 2022), regularization terms (Akhound-
 754 Sadegh et al., 2023; Zhang et al., 2023; Dalton et al., 2024), and self-supervised learning (Mialon
 755 et al., 2023). Strictly enforcing symmetry is also possible, but is often restricted to specific symmetries

756 and systems (Wang et al., 2021; Gurevich et al., 2024). For more general symmetries and physical
 757 systems, enforcing symmetry often requires additional assumptions on the form of equations, such as
 758 the linear combination form in sparse regression (Otto et al., 2023; Yang et al., 2024). **EquivSINDy**
 759 ([Yang et al., 2024](#)) has a similar goal to ours: to enforce symmetry when discovering differential
 760 equations. However, they addressed the discovery of first-order autonomous ODE systems, where
 761 they only considered the time-independent symmetries of ODEs (represented in vector fields by
 762 $\sum_i \phi_i(\mathbf{u})\partial_i$). In comparison, we deal with PDEs that contain partial derivatives and possibly higher-
 763 order derivatives, and possibly have no “linear form” assumed by SINDy. In this context, we consider
 764 the general Lie point symmetries of PDEs, which could act on the independent variables nontrivially
 765 (represented in vector fields by $\sum_i \xi_i(\mathbf{x}, \mathbf{u})\partial_{x_i} + \sum_j \phi_j(\mathbf{x}, \mathbf{u})\partial_{u_j}$). To the best of our knowledge,
 766 our work is the first attempt to strictly enforce general symmetries of differential equations for general
 767 symbolic regression methods.

768
 769
 770
 771
 772
 773
 774
 775
 776
 777
 778
 779
 780
 781
 782
 783
 784
 785
 786
 787
 788
 789
 790
 791
 792
 793
 794
 795
 796
 797
 798
 799
 800
 801
 802
 803
 804
 805
 806
 807
 808
 809

810 **B MATH**
811812 **B.1 NOTATIONS**
813814
815
816 Table 2: Descriptions of symbols used throughout the paper. The three blocks include (1) basic
817 notations for PDEs, (2) notations for Lie symmetry of PDEs, and (3) notations for symbolic regression
818 algorithms and miscellaneous.
819

820 Symbols	821 Descriptions
822 p	823 Number of independent variables of a PDE.
824 q	825 Number of dependent variables of a PDE.
826 X	827 Space of independent variables of a PDE: $X \subset \mathbb{R}^p$. Also used to denote the feature 828 space of SR algorithms.
829 U	830 Space of dependent variables of a PDE: $U \subset \mathbb{R}^q$. Assumed to be 1-dimensional 831 unless otherwise stated.
832 E	833 Total space of all variables of a PDE: $E = X \times U$.
834 U_k	835 Space of strictly k th-order partial derivatives of variables in U w.r.t variables in X .
836 $U^{(n)}$	837 Space of all partial derivatives up to n th order (including the original variables in U): 838 $U^{(n)} = U \times U_1 \times \dots \times U_n$.
839 $M^{(n)}$	840 n th-order jet space: $M^{(n)} \subset X \times U^{(n)}$.
841 $T\mathcal{M}$	842 The tangent bundle of a manifold \mathcal{M} .
843 \mathbf{x}	844 Independent variables of a PDE: $\mathbf{x} \in \mathbb{R}^p$.
845 t	846 Time variable.
847 x, y	848 Spatial variables in PDE contexts. Also used to denote the features and labels of SR 849 algorithms, where x can denote multi-dimensional features.
850 u, \mathbf{u}	851 Dependent variable(s) of a PDE: $u \in \mathbb{R}$ and $\mathbf{u} \in \mathbb{R}^q$.
852 $u^{(n)}, \mathbf{u}^{(n)}$	853 The collection of all up to n -th order partial derivatives of u or \mathbf{u} .
854 df	855 The (ordinary) differential of a function. For a differential function $f : M^{(n)} \rightarrow \mathbb{R}$, 856 $df = \sum_j \frac{\partial f}{\partial x^j} dx^j + \sum_\alpha \frac{\partial f}{\partial u_\alpha} du_\alpha$.
857 $D_i f$	858 The total derivative of a differential function $f : M^{(n)} \rightarrow \mathbb{R}$ w.r.t the i th independent 859 variable. For example, if $p = q = 1$, $D_1 f = \frac{\partial f}{\partial x} + \sum_{k=0}^{\infty} u_{k+1} \frac{\partial f}{\partial u_k}$, where $u_k :=$ 860 $\partial^k u / \partial x^k$.
861 Df	862 The total differential of a differential function $f : M^{(n)} \rightarrow \mathbb{R}$, i.e. $Df = D_i f dx^i$.
863 g	864 A group element with an action on E (2).
865 \mathbf{v}	866 A vector field on the total space E (3), representing an infinitesimal transformation.
867 $\text{pr}^{(n)} g$	868 A list of multiple vector fields are indexed by subscripts.
869 $\text{pr}^{(n)} \mathbf{v}$	870 n th-order prolongation of g acting on $M^{(n)}$.
871 $g^{(n)}, \mathbf{v}^{(n)}$	872 n th-order prolongation of \mathbf{v} acting on $M^{(n)}$.
873 $\text{pr } \mathbf{v}$	874 Equivalent to $\text{pr}^{(n)} g$ and $\text{pr}^{(n)} \mathbf{v}$, respectively.
875 η, ζ, ϑ	876 The (infinite) prolongation of \mathbf{v} . For an n th-order differential function $f(\mathbf{x}, \mathbf{u}^{(n)})$, 877 $\text{pr } \mathbf{v}(f) = \text{pr}^{(n)} \mathbf{v}(f)$.
878 ℓ, ℓ	879 Differential invariants of a symmetry group. η is used by default. The other letters 880 are used to distinguish between invariants of different orders.
881 θ	882 The LHS of SINDy equation (4). Often assumed to be time derivatives.
883 \mathbf{w}, W	884 A column vector containing all SINDy library functions: $\theta = [\theta^1, \dots, \theta^m]$
885 \mathbf{X}, \mathbf{y}	886 The SINDy parameters. For only one equation, $\mathbf{w} = [w^1, \dots, w^m]$ is a row vector. 887 For multiple equations, $W = [w^{ij}]$ is a $q \times m$ matrix.
888 $[N]$	889 Concatenated matrix/vector of features/labels of all datapoints for symbolic regression.
889 $1 : N$	890 List of positive integers up to N , i.e. $[1, 2, \dots, N]$ for any $N \in \mathbb{Z}^+$.
891 LHS, RHS	892 Equivalent to $[N]$.
893	894 Left- and Right-hand side of an equation.

864 B.2 EXTENDED BACKGROUND ON PDE SYMMETRY
865866 References for the below material include Olver (1993), Olver (1995).
867868 **Prolonged group actions** Let $E = X \times U \simeq \mathbb{R}^p \times \mathbb{R}^q$ be endowed with the action of a group G via
869 point transformations. Then group elements $g \in G$ act locally on functions $\mathbf{u} = f(\mathbf{x})$, therefore also
870 on derivatives of these functions. This in turn induces, at least pointwise, “prolonged” transformations
871 on jet spaces: $(\tilde{\mathbf{x}}, \tilde{\mathbf{u}}^{(n)}) = \text{pr}^{(n)} g \cdot (\mathbf{x}, \mathbf{u}^{(n)})$.
872873 Let $J = (j_1, \dots, j_n)$, $1 \leq j_\nu \leq p$ be an n -tuple of indices of independent variables and $1 \leq \alpha \leq q$.
874 We will use the shorthand

874
$$u_J^\alpha := \frac{\partial^J u^\alpha}{\partial x^J} := \frac{\partial^{|J|} u^\alpha}{\partial x_{j_1} \cdots \partial x_{j_n}}$$

875

876 and

877
$$D_J := D_{j_1} \cdots D_{j_n}.$$

878

879 It is not practical to work explicitly with prolonged group transformations. Therefore one linearizes
880 and considers the prolonged action of the infinitesimal generators of G . Explicitly, given a vector
881 field

882
$$\mathbf{v} = \sum_{i=1}^p \xi^i(\mathbf{x}, \mathbf{u}) \frac{\partial}{\partial x^i} + \sum_{\alpha=1}^q \varphi^\alpha(\mathbf{x}, \mathbf{u}) \frac{\partial}{\partial u^\alpha},$$

883

884 its **characteristic** is a q -tuple $Q = (Q^1, \dots, Q^q)$ of functions with
885

886
$$Q^\alpha(\mathbf{x}, \mathbf{u}^{(1)}) = \varphi^\alpha(\mathbf{x}, \mathbf{u}) - \sum_{i=1}^p \xi^i(\mathbf{x}, \mathbf{u}) \frac{\partial u^\alpha}{\partial x^i}.$$

887

888 Now the prolongation of \mathbf{v} to order n is defined by
889

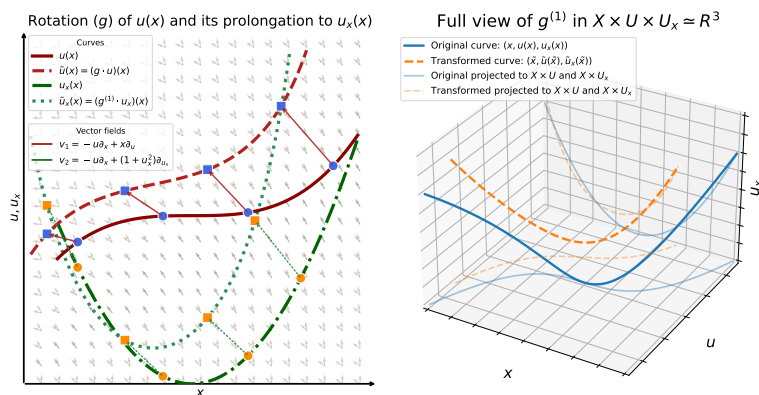
890
$$\text{pr}^{(n)} \mathbf{v} = \sum_{i=1}^p \xi^i(\mathbf{x}, \mathbf{u}) \frac{\partial}{\partial x^i} + \sum_{\alpha=1}^q \sum_{\#J=n} \varphi_J^\alpha(\mathbf{x}, \mathbf{u}^{(n)}) \frac{\partial}{\partial u_J^\alpha}. \quad (9)$$

891

892 Here J ranges over all n -tuples $J = (j_1, \dots, j_n)$, $1 \leq j_\nu \leq p$ and the φ_J^α are given by
893

894
$$\varphi_J^\alpha = D_J Q^\alpha + \sum_{i=1}^p \xi^i \mathbf{u}_{J,i}^\alpha.$$

895

896 We remark that the prolongation of \mathbf{v} has been described explicitly in terms of the coefficients of \mathbf{v}
897 and their derivatives.914 Figure 4: Demonstration of the rotation $\mathbf{v} = -u \partial_x + x \partial_u$ acting on $X \times U$, and its first-order
915 prolongation acting on $X \times U \times U_1$.916 Figure 4 visualizes the group action of a Lie point transformation and its prolongation with a simple
917 example. Consider the total space $X \times U \simeq \mathbb{R} \times \mathbb{R}$, and the standard rotation generator in 2D space

given by $\mathbf{v} = -u\partial_x + x\partial_u$. The vector field is visualized in dark red arrows in the background. We also consider a function $X \rightarrow U$ given by $u(x) = 0.5(x - 1)^3$, whose graph is visualized by the dark red solid line in Figure 4 left. The graph of its first-order derivative, $u_x(x) = 1.5(x - 1)^2$, is visualized by the dark green dash-dot line.

Then, we choose a random group element $g = \exp(\theta\mathbf{v})$ that rotates a 2D vector $(x, u) \in X \times U$ by angle θ . Applying this pointwise transformation to every point on the graph of $u(x)$, we have a transformed graph visualized by the dark red dashed line. The transformed function, $\tilde{u} = g \cdot u$, is defined as the function whose graph is the transformed graph. In other words, $\tilde{u}(x) = (g \cdot u)(x)$ is visualized by the dark red dashed line in Figure 4 left.

Next, we consider how the rotation of (x, u) transforms the first-order derivative $u_x := \frac{du}{dx}$. The prolonged vector field, i.e., the infinitesimal generator of the prolonged group action, can be computed by (9): $\mathbf{v}^{(1)} = \mathbf{v} + (1 + u_x^2)\partial_{u_x}$. The projection of $\mathbf{v}^{(1)}$ onto $X \times U_1$ is visualized in the dark green arrows in Figure 4 left. Similarly, the prolonged group action $g^{(1)} = \exp(\theta\mathbf{v}^{(1)})$ is applied to every point on the graph of $u_x(x)$, yielding the graph of the transformed derivative function, $\tilde{u}_x(x) = \frac{d\tilde{u}}{dx}(x)$, visualized in the dark green dotted line.

The full transformation of the prolonged $g^{(1)}$ in the 3D space $X \times U \times U_1$ is shown on Figure 4 right. The graph of the original prolonged function $u^{(1)}(x) = (u(x), u_x(x))$ is shown in the solid line, which is transformed into the dashed line by $g^{(1)}$.

B.3 PROOF OF PROPOSITION 3.3

Olver (1995) provides the following general theorem to construct higher-order differential invariants from a contact-invariant coframe. We refer the readers to Chapter 5 of Olver (1995) for definitions of relevant concepts, e.g., contact forms and contact-invariant forms and coframes.

Theorem B.1 (Thm. 5.48, (Olver, 1995)). *Let G be a transformation group acting on a space with p independent variables and q dependent variables. Suppose $\omega^1, \dots, \omega^p$ is a contact-invariant coframe for G , and let D_j be the associated invariant differential operators defined via $Df = D_j f dx^j = D_j f \omega^j$. If there are a e number of independent, strictly n th-order differential invariants $\zeta^1, \dots, \zeta^{q_n}$, $q_n = \binom{p+n-1}{n}$, then the set of differentiated invariants $D_i \zeta^\nu$, $i \in [p]$, $\nu \in [q_n]$, contains a complete set of independent, strictly $(n+1)$ th-order differential invariants.*

Specifically, the condition that there exist a maximal number of differential invariants of order exactly n is guaranteed if n is at least $\dim G$.

Our proposition is a derived result from the above theorem, which provides a concrete way of computation from lower-order invariants to higher-order ones:

Proposition B.2. *Let G be a local group acting on $X \times U \simeq \mathbb{R}^p \times \mathbb{R}$. Let $\eta^1, \eta^2, \dots, \eta^p$ be any p differential invariants of G whose horizontal Jacobian $J = [D_i \eta^j]$ is non-degenerate on an open subset $\Omega \subset M^{(n)}$. If there are a maximal number of independent, strictly n th-order differential invariants $\zeta^1, \dots, \zeta^{q_n}$, $q_n = \binom{p+n-1}{n}$, then the following set contains a complete set of independent, strictly $(n+1)$ th-order differential invariants defined on Ω :*

$$\frac{\det(D_i \tilde{\eta}_{(k, k')}^j)}{\det(D_i \eta^j)}, \quad \forall k \in [p], k' \in [q_n], \quad (10)$$

where $i, j \in [p]$ are matrix indices, D_i denotes the total derivative w.r.t i -th independent variable and $\tilde{\eta}_{(k, k')}^j = [\eta^1, \dots, \eta^{k-1}, \zeta^{k'}, \eta^{k+1}, \dots, \eta^p]$.

Proof. We show that the total differentials of the differential invariants η^1, \dots, η^p can be used to construct a *contact-invariant coframe* of G and then derive the associated invariant differential operators to complete the proof.

First, note that for any differential invariant η of G , its total differential $\omega = D\eta = D_j \eta dx^j$ can be written as

$$\omega = \omega_o + \theta, \quad (11)$$

972 where $\omega_o := d\eta = \sum_{i \in [p]} \frac{\partial F}{\partial x^i} dx^i + \sum_{|\alpha| \leq n} \frac{\partial F}{\partial u_\alpha} du_\alpha$ is the ordinary differential of $\eta : M^{(n)} \rightarrow \mathbb{R}$
 973 and θ is a contact form.
 974

975 Since η is a differential invariant, its differential $\omega_o = d\eta$ is an invariant one-form on $M^{(n)}$, i.e.
 976 $(g^{(n)})^* \omega_o = \omega_o$.

977 Also, a prolonged group action maps contact forms to contact forms. To see this, note that a prolonged
 978 group action $g^{(n)}$ maps the prolonged graph of any function to the prolonged graph of a transformed
 979 function. Then, for any contact form θ , $(g^{(n)})^* \theta$ is annihilated by all prolonged functions $f^{(n)}$, thus
 980 a contact form by definition:

$$\begin{aligned} 981 \quad (f^{(n)})^*((g^{(n)})^* \theta) &= (g^{(n)} \circ f^{(n)})^* \theta \\ 982 \quad &= ((g \cdot f)^{(n)})^* \theta \\ 983 \quad &= 0. \end{aligned} \tag{12}$$

984 Then, from (11), we have
 985

$$\begin{aligned} 986 \quad (g^{(n+1)})^* \omega &= (g^{(n)})^* \omega_o + (g^{(n+1)})^* \theta \\ 987 \quad &= \omega_o + \theta' \\ 988 \quad &= \omega + (\theta' - \theta) \end{aligned} \tag{13}$$

989 where θ' is some contact form and so is $\theta' - \theta$. Thus, ω is contact-invariant. For the p differential
 990 invariants η^1, \dots, η^p , we have p contact-invariant one-forms $\omega^1, \dots, \omega^p$, respectively.
 991

992 Next, we prove that $\omega^1, \dots, \omega^p$ are linearly independent and form a coframe. Assume there exists
 993 smooth coefficients c^j such that $\sum_j c^j \omega^j = 0$. Then, regrouping the coefficients of the horizontal
 994 forms dx^i , we have
 995

$$0 = \sum_{i,j} c^j D_i \eta^j dx^i = \sum_i \left(\sum_j c^j D_i \eta^j \right) dx^i. \tag{14}$$

1001 Because the dx^i are linearly independent, each coefficient of dx^i must vanish, i.e. $J_i^j c^j = 0$.
 1002 Since the Jacobian $J = [D_i \eta^j]$ is non-degenerate, the only solution is $c^j = 0$ (on the open subset
 1003 $\Omega \in M^{(n)}$). Thus, $\omega^1, \dots, \omega^p$ form a contact-invariant coframe. According to Theorem B.1, the
 1004 associated invariant differential operators of the coframe take a complete set of same-order invariants
 1005 to a complete set of one-order-higher invariants.
 1006

1007 The remaining step is to obtain the invariant differential operators explicitly in terms of η^j . Recall
 1008 the formula in Theorem B.1 that defines the invariant differential operators:
 1009

$$D_i f dx^i = \mathcal{D}_j f \omega^j. \tag{15}$$

1010 Expanding $\omega^j = D\eta^j = D_i \eta^j dx^i$, we have the following linear system of invariant differential
 1011 operators \mathcal{D}_j :

$$\begin{bmatrix} D_1 \\ D_2 \\ \vdots \\ D_p \end{bmatrix} = \begin{bmatrix} D_1 \eta^1 & D_1 \eta^2 & \cdots & D_1 \eta^p \\ D_2 \eta^1 & D_2 \eta^2 & \cdots & D_2 \eta^p \\ \vdots & \vdots & & \vdots \\ D_p \eta^1 & D_p \eta^2 & \cdots & D_p \eta^p \end{bmatrix} \begin{bmatrix} \mathcal{D}_1 \\ \mathcal{D}_2 \\ \vdots \\ \mathcal{D}_p \end{bmatrix}. \tag{16}$$

1018 Since $J = [D_i \eta^j]$ is non-degenerate, Cramer's rule yields
 1019

$$\mathcal{D}_k \zeta = \frac{\det(D_i \eta^1 \mid \cdots \mid D_i \eta^{k-1} \mid D_i \zeta \mid D_i \eta^{k+1} \mid \cdots \mid D_i \eta^p)}{\det(D_i \eta^j)}. \tag{17}$$

1020 \square
 1021

1022 **Remark B.3.** We require that the differential invariants η^1, \dots, η^p has a nondegenerate horizontal
 1023 Jacobian $[D_i \eta^j]$, which is a stronger condition than functional independence. Since the differential
 1024

invariants are functions on the jet space, it is possible that a set of such functions is functionally independent, i.e., has a nondegenerate full Jacobian $[\partial_i \eta^j]$, where $i \in [q_n]$ indexes the jet space variables $(\mathbf{x}, u^{(n)})$, but has a lower-rank horizontal Jacobian. For example, consider $\eta^1 = u_x$ and $\eta^2 = u_y$. In the full Jacobian, $\partial \eta^j / \partial u_x$ and $\partial \eta^j / \partial u_y$ form the identity, so it has full rank. However, its horizontal Jacobian containing total derivatives is given by $\begin{bmatrix} u_{xx} & u_{xy} \\ u_{xy} & u_{yy} \end{bmatrix}$, which is not invertible on the subset of the jet space where $u_{xx}u_{yy} - u_{xy}^2 = 0$.

In practice, this non-degeneracy condition can be easily checked once we have the symbolic expressions of the p differential invariants.

Remark B.4. When $p = 1$, Proposition B.2 is equivalent to the following (Prop. 2.53, Olver (1993)):

If $y = \eta(x, u^{(n)})$ and $w = \zeta(x, u^{(n)})$ are n -th order differential invariants of G , then $\frac{dw}{dy} \equiv \frac{D_x \zeta}{D_x \eta}$ is an $(n+1)$ -th order differential invariant of G . Specifically, if $y = \eta(x, u)$ and $w = \zeta(x, u, u_x)$ form a complete set of functionally independent differential invariants of $\text{pr}^{(1)}G$, the complete set of functionally independent differential invariants for $\text{pr}^{(n)}G$ is then given by

$$y, w, dw/dy, \dots, d^{n-1}w/dy^{n-1}. \quad (18)$$

B.4 EXAMPLES OF COMPUTING DIFFERENTIAL INVARIANTS

Example B.5. Consider the group $\text{SO}(2)$ acting on $X \times U \simeq \mathbb{R}^2 \times \mathbb{R}$ by standard rotation in the 2D space of independent variable and trivial action on U , i.e. its infinitesimal generator given by $\mathbf{v} = y\partial_x - x\partial_y$.

First, we solve for a complete set of the ordinary and first-order invariants. By definition, the ordinary invariants $\eta = \eta(x, y, u)$ should satisfy $y\partial_x \eta - x\partial_y \eta = 0$. Since the vector field does not involve u , an immediate solution is $\eta = u$. On the other hand, by method of characteristics, we convert the PDE to the characteristic equations $dx/ds = y, dy/ds = -x$. That is, the characteristics curves $(x(s), y(s))$ are just circles around origin. Because η is constant along characteristic curves, it must be a function of $R^2 = x^2 + y^2$. Therefore, we pick the following two ordinary invariants: $\eta_1(x, y, u) = \frac{1}{2}(x^2 + y^2)$ and $\eta_2(x, y, u) = u$. (5) dictates how we construct higher-order invariants using these two functionally independent invariants and another arbitrary invariant. For notational convenience, we convert (5) to operators defined according to η_2 and η_1 , respectively:

$$\mathcal{O}_1 = \frac{x D_y - y D_x}{x u_y - y u_x} \quad (19)$$

$$\mathcal{O}_2 = \frac{u_y D_x - u_x D_y}{x u_y - y u_x} \quad (20)$$

Then, we need to find another new differential invariant, because applying these operators on η_1 and η_2 leads to trivial results. Since η_1 and η_2 generate all ordinary (zeroth-order) invariants, we must look for the first-order invariants. To do this, note the prolonged vector field is given by

$$\text{pr}^{(1)}\mathbf{v} = \mathbf{v} + u_y \partial_{u_x} - u_x \partial_{u_y} \quad (21)$$

Solving for $\text{pr}^{(1)}\mathbf{v}$ gives two first-order invariants, $\zeta_1 = x u_y - y u_x$ and $\zeta_2 = x u_x + y u_y$. Note that the differential invariant ζ_1 is exactly the common denominator in \mathcal{O}_1 and \mathcal{O}_2 , so we can simplify \mathcal{O}_1 and \mathcal{O}_2 by using only their numerators, i.e.

$$\mathcal{O}_1 = x D_y - y D_x \quad (22)$$

$$\mathcal{O}_2 = u_y D_x - u_x D_y \quad (23)$$

Note that \mathcal{O}_2 has first-order coefficients, which may complicate things in the subsequent calculation. Denoting the space of all continuous functions of the existing four invariants as $\mathcal{I} = \mathcal{C}(\eta_1, \eta_2, \zeta_1, \zeta_2)$, we can choose any new operator within the \mathcal{I} -module spanned by \mathcal{O}_1 and \mathcal{O}_2 that makes things easier. Specifically, we use the following operator

$$\begin{aligned} \tilde{\mathcal{O}}_2 &= \frac{\zeta_2}{\zeta_1} \mathcal{O}_1 + \frac{2\eta_1}{\zeta_1} \mathcal{O}_2 \\ &= x D_x + y D_y \end{aligned} \quad (24)$$

1080 Then, we apply these operators to the first-order invariants, which raise the order by one and give us
 1081 the second-order invariants. For example, applying \mathcal{O}_1 to ζ_1 , we have
 1082

$$\begin{aligned} \mathcal{O}_1 \zeta_1 &= x D_y \zeta_1 - y D_x \zeta_1 \\ &= x(xu_{yy} - u_x - yu_{xy}) - y(u_y + xu_{xy} - yu_{xx}) \\ &= x^2 u_{yy} + y^2 u_{xx} - xu_x - yu_y - 2xyu_{xy} \end{aligned} \quad (25)$$

1087 Note that $\zeta_2 = xu_x + yu_y$ is a first-order invariant, so we can further remove it from the formula and
 1088 get a simplified second-order invariant
 1089

$$\vartheta_1 = x^2 u_{yy} + y^2 u_{xx} - 2xyu_{xy} \quad (26)$$

1091 Similarly, we compute $\mathcal{O}_1 \zeta_2$, $\tilde{\mathcal{O}}_2 \zeta_1$ and $\tilde{\mathcal{O}}_2 \zeta_2$ and obtain the following, respectively:
 1092

$$\begin{aligned} \vartheta_2 = \vartheta_3 &= \zeta_1 + xy(u_{yy} - u_{xx}) + (x^2 - y^2)u_{xy} \\ &\equiv xy(u_{yy} - u_{xx}) + (x^2 - y^2)u_{xy} \end{aligned} \quad (27)$$

$$\begin{aligned} \vartheta_4 &= \zeta_2 + x^2 u_{xx} + y^2 u_{yy} + 2xyu_{xy} \\ &\equiv x^2 u_{xx} + y^2 u_{yy} + 2xyu_{xy} \end{aligned} \quad (28)$$

1098 The above 8 invariants should form a complete set of second-order differential invariants of $\mathbf{v} =
 1099 x\partial_y - y\partial_x$. To verify, note that the Laplacian $\Delta u = u_{xx} + u_{yy}$, which is a well-known rotational
 1100 invariant, can be written in terms of these differential functions:

$$\begin{aligned} \Delta u = u_{xx} + u_{yy} &= \frac{(x^2 + y^2)(u_{xx} + u_{yy})}{x^2 + y^2} \\ &= \frac{\vartheta_1 + \vartheta_4}{2\eta_1} \end{aligned} \quad (29)$$

1106 Another second-order rotational invariant, the trace of the squared Hessian matrix, $u_{xx}^2 + 2u_{xy}^2 + u_{yy}^2$,
 1107 is recovered by
 1108

$$u_{xx}^2 + 2u_{xy}^2 + u_{yy}^2 = \frac{\vartheta_1^2 + 2\vartheta_2^2 + \vartheta_4^2}{4\eta_1^2} \quad (30)$$

1111 On the other hand, these 8 invariants are apparently not functionally independent - note that $\vartheta_2 =
 1112 \mathcal{O}_1 \zeta_2$ and $\vartheta_3 = \tilde{\mathcal{O}}_2 \zeta_1$ are the same. While this may be some coincidence, eventually it is not surprising
 1113 because we would expect to see 3 functionally independent strictly second-order differential invariants
 1114 instead of 4, since $(u_{xx}, u_{yy}, u_{xy}) \in U_2$ is only 3-dimensional.

1115 *Example B.6 (Scaling and translation).* Consider the vector field $\mathbf{v}_1 = t\partial_t + ax\partial_x + bu\partial_u$. It generates
 1116 the scaling symmetry $t \mapsto \lambda t, x \mapsto \lambda^a x, u \mapsto \lambda^b u$. The ordinary invariants of this symmetry are
 1117 $t^b u^{-1}$ and $x^a u^{-1}$. The higher-order invariants are given by $\eta_{(\alpha, \beta)} = x^\alpha t^\beta u_{x^{(\alpha)} t^{(\beta)}} u^{-1}$, where α and
 1118 β denote the orders of partial derivatives w.r.t t and x , e.g. $u_{x^{(2)} t^{(1)}} := u_{xxt}$.

1119 Besides the scaling symmetry, we can consider other common symmetries simultaneously, e.g.
 1120 translation symmetries in both space and time, $\mathbf{v}_2 = \partial_x$ and $\mathbf{v}_3 = \partial_t$. These symmetries, along with
 1121 the scaling symmetry \mathbf{v}_1 , span a three-dimensional symmetry group. There are no ordinary invariants
 1122 due to the translation symmetries. A convenient maximal set of functionally independent differential
 1123 invariants is given by
 1124

$$\eta_{(\alpha, \beta)} = u_{x^{(\alpha)} t^{(\beta)}} u_x^{\frac{b-a\alpha-\beta}{a-b}}, \quad \alpha \geq 0, \beta \geq 0. \quad (31)$$

1125 B.5 PROOF OF PROPOSITION 3.4

1127 Proposition 3.4, restated below, aligns our symmetry constraint into the SINDy framework and results
 1128 in a set of constraints on the SINDy parameters.
 1129

1130 **Proposition B.7.** *Let $\ell(\mathbf{x}, \mathbf{u}^{(n)}) = W\boldsymbol{\theta}(\mathbf{x}, \mathbf{u}^{(n)})$ be a system of q differential equations admitting a
 1131 symmetry group G , where $\mathbf{x} \in \mathbb{R}^p$, $\mathbf{u} \in \mathbb{R}^q$, $\boldsymbol{\theta} \in \mathbb{R}^m$. Assume there exist some n th-order invariants
 1132 of G , $\eta_0^{1:q}$ and $\eta^{1:K}$, s.t. (1) the system of equations can be expressed as $\eta_0 = W' \boldsymbol{\theta}'(\boldsymbol{\eta})$, where
 1133 $\eta_0 = [\eta_0^{1:q}]$ and $\boldsymbol{\eta} = [\eta^{1:K}]$, and (2) $\eta_0^i = T^{ijk} \theta^k \ell^j$ and $(\boldsymbol{\theta}')^i = S^{ij} \theta^j$, for some functions $\boldsymbol{\theta}'(\boldsymbol{\eta})$
 and constant tensors W' , T and S . Then, the space of all possible W is a linear subspace of $\mathbb{R}^{q \times m}$.*

1134 *Proof.* (Note: In this proof, we do not distinguish between superscripts and subscripts. All are used
 1135 for tensor indices, not partial derivatives.)

1136 For simplicity, we omit the dependency of functions and write

$$1138 \quad \ell^i = W^{ij} \theta^j. \quad (32)$$

1140 Combining the conditions about the differential invariants, we know that the equation can be equiva-
 1141 lently expressed as

$$1142 \quad T^{ijk} \theta^k \ell^j = (W')^{ij} S^{jk} \theta^k \quad (33)$$

1143 for some $W' \in \mathbb{R}^{q \times m'}$, where m' is the number of invariant functions in θ' .

1144 Substituting (32) into (33) and rearranging the indices, the principle of symmetry invariants then
 1145 translates to the following constraint on W : there exists some $W' \in \mathbb{R}^{q \times m'}$ s.t.

$$1147 \quad T_i^{rk} \theta_k W_r^l \theta_l = (W')_i^k S_k^j \theta_j, \forall \mathbf{x}, \mathbf{u}^{(n)}. \quad (34)$$

1149 To solve for W , we first eliminate the dependency on the variables \mathbf{x} and $\mathbf{u}^{(n)}$ from the equation.
 1150 We adopt a procedure similar to Yang et al. (2024). Denote $\mathbf{z} = (\mathbf{x}, \mathbf{u}^{(n)})$. Define a functional
 1151 M_{θ} as mapping a function to its coordinate in the function space spanned by θ , i.e. $M_{\theta} : (\mathbf{z} \mapsto$
 1152 $c^j \theta_j(\mathbf{z})) \mapsto (c^1, c^2, \dots, c^m)$. Before we proceed, note that the LHS of (34) contains the products of
 1153 functions $\theta_k(\mathbf{z}) \theta_l(\mathbf{z})$, which may or may not be included in the original function library θ . Therefore,
 1154 we denote $\tilde{\theta}(\mathbf{z}) = [\theta(\mathbf{z}) \mid \{\theta_k \theta_l \notin \theta\}]$ as the collection of all library functions θ_k and all their
 1155 products $\theta_k \theta_l$. The invariant functions $\theta'(\eta)$ can also be rewritten in terms of the prolonged library:
 1156 $\theta'(\eta) = \tilde{S} \tilde{\theta}$, where $\tilde{S}_{1:m} = S$.

1158 Then, applying $M_{\tilde{\theta}}$ to (34), we have

$$1160 \quad M_{\tilde{\theta}}(T_i^{rk} \theta_k W_r^l \theta_l) = (W')_i^k \tilde{S}_k^j. \quad (35)$$

1162 Further expanding the LHS, we have

$$1163 \quad T_i^{rk} W_r^l \Gamma_{kl}^j = (W')_i^k \tilde{S}_k^j, \quad (36)$$

1165 where Γ satisfies $\theta_k \theta_l = \Gamma_{kl}^j \tilde{\theta}_j$. In other words, the rows of the LHS fall in the row space of \tilde{S} . Let
 1166 \tilde{S}^\perp be the basis matrix for the null space of \tilde{S} , i.e. $\tilde{S} \tilde{S}^\perp = 0$, we have

$$1168 \quad T_i^{rk} W_r^l \Gamma_{kl}^j (\tilde{S}^\perp)_{js} = 0, \quad (37)$$

1170 suggesting that W must lie in a linear subspace of $\mathbb{R}^{q \times m}$.

1171 \square

1172 *Remark B.8.* In practice, to solve for (37), we first rearrange (37) into $M \text{vec}(W) = 0$, where M
 1173 has shape $(\tilde{S}.\text{shape}[2] \times q, q \times m)$. Then, we perform SVD on M and apply a threshold of 10^{-6} to
 1174 the singular values. The right singular vectors corresponding to the singular values smaller than the
 1175 threshold then form a basis of the linear subspace $\text{vec}(W)$ lies in.

1177 C IMPLEMENTATION DETAILS

1180 This section discusses some detailed considerations in implementing the sparse regression-based
 1181 methods described in Section 3.3 and 3.4. Contents include:

- 1182 • Appendix C.1: An algorithmic description of direct sparse regression with symmetry
 1183 invariants.
- 1184 • Appendix C.2: Converting the symmetry invariant condition as linear constraints on the
 1185 sparse regression parameters.
- 1186 • Appendix C.3: Using differential invariants in weak SINDy via the linear constraints, as
 1187 well as other considerations.

1188
1189

C.1 DIRECT SPARSE REGRESSION WITH SYMMETRY INVARIANTS

1190
1191
1192
1193
1194
1195
1196
1197

The first approach to enforcing symmetry in sparse regression, as discussed in Section 3.3, is to directly use the symmetry invariants as the variables and their functions specified by a function library as the RHS features. Similar to Algorithm 1 for general symbolic regression methods, we provide a detailed algorithm for sparse regression below. Following the setup from SINDy, we aim to discover a system of q differential equations for q dependent variables.

1198
1199
1200
1201
1202
1203
1204
1205
1206
1207**Algorithm 2** Sparse regression with symmetry invariants

Require: PDE order n , dataset $\{\mathbf{z}^i = (\mathbf{x}^i, (\mathbf{u}^{(n)})^i) \in M^{(n)}\}_{i=1}^{N_D}$, SINDy LHS ℓ , SINDy function library $\{\theta^j\}$, infinitesimal generators of the symmetry group $\mathcal{B} = \{\mathbf{v}_a\}$.

Ensure: A PDE system admitting the given symmetry group.

Compute the symmetry invariants of \mathcal{B} up to n th-order: η^1, \dots, η^K . {Prop. 3.3}

Choose an invariant function η^{k_i} s.t. $\partial\eta^{k_i}/\partial\ell^i \neq 0$ for SINDy LHS component ℓ^i .

Let $\boldsymbol{\eta}_0 = [\eta^{k_1}, \dots, \eta^{k_q}]^T$ and $\boldsymbol{\eta}$ denote the column vector containing the remaining $K - q$ invariants.

Instantiate the sparse regression model as $\boldsymbol{\eta}_0 = W\boldsymbol{\theta}(\boldsymbol{\eta})$.

Optimize W with the SINDy objective: $\sum_i \|\boldsymbol{\eta}_0(\mathbf{z}^i) - W\boldsymbol{\theta}(\boldsymbol{\eta}(\mathbf{z}^i))\|^2 + \lambda\|W\|_0$.

return $\boldsymbol{\eta}_0 = W\boldsymbol{\theta}(\boldsymbol{\eta})$. {Optionally, expand all η^j in terms of original variables \mathbf{z} .}

1208
1209
1210
1211
1212
1213
1214
1215
1216
1217

The configuration from the original SINDy model, i.e., the LHS ℓ and the function library $\{\theta^j\}$, are used to construct a new equation model in terms of the invariants. It should be noted that the functions in the SINDy function library does not specify their input variables. For example, in the PySINDy (Kaptanoglu et al., 2022) implementation, a function θ is provided in a lambda format `lambda x, y: x * y`. Thus, θ can be applied to both the original variables, e.g. $\theta(z_1, z_2) = z_1 z_2$, and the invariant functions, e.g. $\theta(\eta_1, \eta_2) = \eta_1 \eta_2$.

C.2 SYMMETRY INVARIANT CONDITION AS LINEAR CONSTRAINTS

1218
1219
1220
1221
1222
1223
1224
1225
1226
1227
1228
1229
1230
1231
1232
1233
1234
1235
1236
1237
1238
1239

Instead of directly using the invariant functions η as the features and labels for regression, we can derive a set of linear constraints from the fact that the equation can be rewritten in terms of invariant functions. As shown in Appendix B.5, a basis Q of the constrained parameter space can be obtained from the right singular vectors of a constraint matrix M . We rearrange Q to a tensor of shape (r, q, m) , where r is the dimension of the constrained parameter space, and (q, m) is the original shape of the parameter matrix W . Then, we can parameterize W by $W^{jk} = Q^{ijk}\beta^i$, where β is the learnable parameter, and discover the equation using the original SINDy objective as described in Section 2.2.

In practice, we observe that the basis Q obtained from SVD is not sparse. Indeed, SVD does not inherently encourage sparsity in the singular vectors. The lack of sparsity can pose a problem when we perform sequential thresholding in sparse regression. Specifically, in SINDy, the entries in W that are close to zero are filtered out at the end of each iteration, which serves as a proxy to the L_0 regularization. Since we fix Q and only optimize β , a straightforward modification to the sequential thresholding procedure is to threshold the entries in β instead of those in W . However, if Q is dense, even a sparse vector β can lead to a dense W , which contradicts the purpose of sparse regression.

Therefore, after performing SVD, we apply a Sparse PCA to Q to obtain a sparsified basis, also of shape (r, q, m) :

```
spca = SparsePCA(n_components=r)
spca.fit(Q.reshape(r, q*m))
Q_sparse = spca.components_.reshape(r, q, m)
```

1240
1241

Figure 5 shows an example of the original basis solved from SVD (top 7×2 grid) and the sparsified basis using sparse PCA (bottom 7×2 grid). This is used in our experiment on the reaction-diffusion system (8).

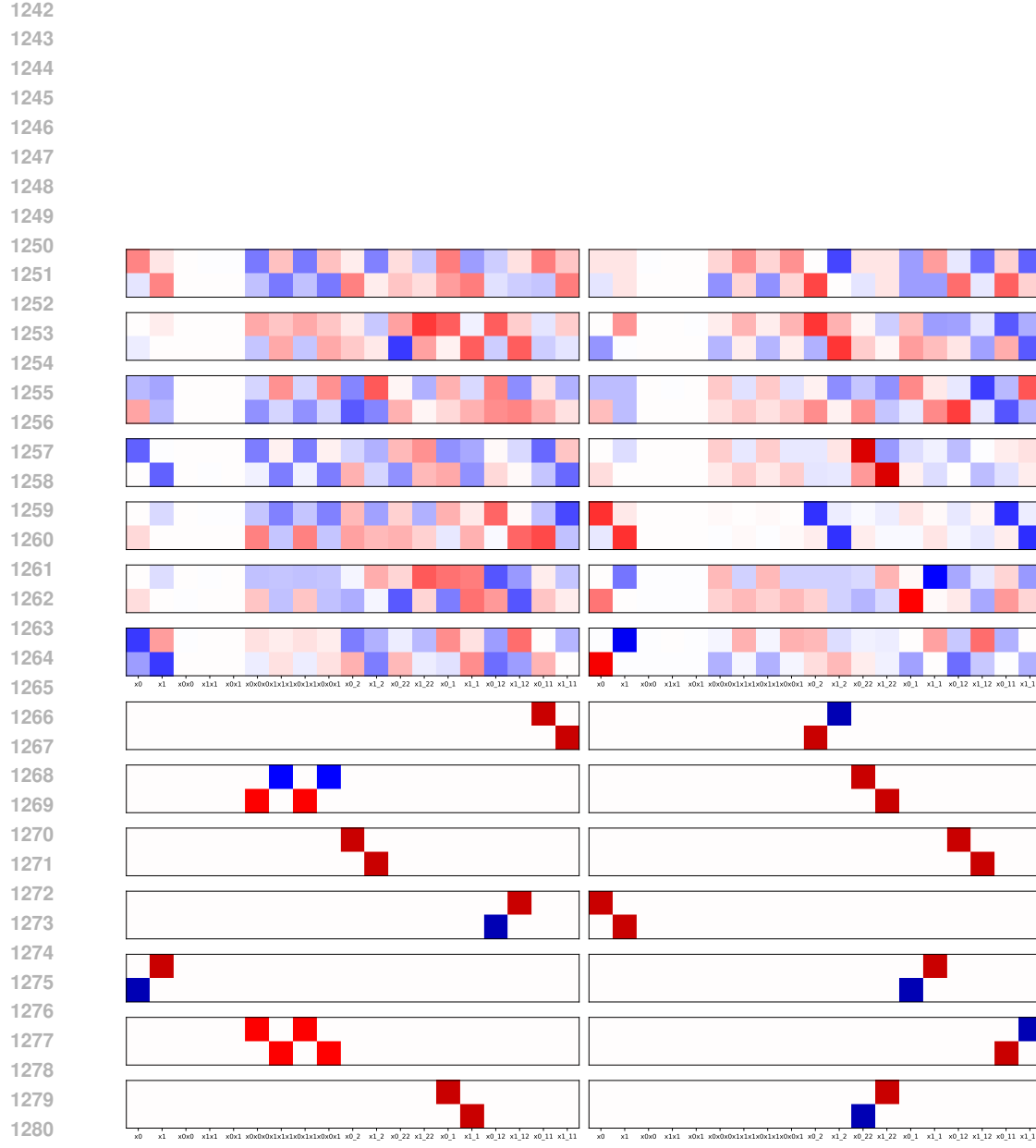


Figure 5: Basis for the SINDy parameter subspace that preserves $\text{SO}(2)$ symmetry $\mathbf{v} = -v\partial_u + u\partial_v$. The SINDy parameter W has dimension 2×19 . The two rows correspond to the two equations with u_t and v_t as the LHSs. The RHS contains 19 features, including all monomials of u, v up to degree 3 and their spatial derivatives up to order 2. The set of symmetry invariants used to compute the basis is given by $\{t, x, y, u^2 + v^2\} \cup \{\mathbf{u} \cdot \mathbf{u}_\mu\} \cup \{\mathbf{u}^\perp \cdot \mathbf{u}_\mu\}$, where $\mathbf{u} = (u, v)^T$ and μ is a multiindex of t, x, y with order no more than 2.

1296 C.3 USING DIFFERENTIAL INVARIANTS IN WEAK SINDY
1297

1298 In this subsection, we discuss the formulation of weak SINDy and how to implement our strategy
1299 of using differential invariants within the weak SINDy framework. To maintain a similar notation
1300 to the original works on weak SINDy (Messenger & Bortz, 2021a;b), we use D_{α_s} to denote partial
1301 derivative operators, where $\alpha_s = (s_1, s_2, \dots, s_p)$ is a multi-index, instead of using subscripts for
1302 partial derivatives. Thus, we no longer strictly differentiate subscripts and superscripts—both can be
1303 used for indexing lists, vectors, etc.

1304 Given a differential equation in the form

$$1306 D_{\alpha_0} u = \sum_{s,j} W_{sj} D_{\alpha_s} f_j(u), \quad (38)$$

1308 we can perform integration by parts (i.e., divergence theorem) to move the derivatives from u to some
1309 analytic test function and thus bypass the need to estimate derivatives numerically. First, we multiply
1310 both sides of (38) by a test function ϕ with compact support $\mathcal{B} \subset X$ and integrate over the spacetime
1311 domain:

$$1312 \int_X D_{\alpha_0} u(\mathbf{x}) \phi(\mathbf{x}) d\mathbf{x} = \sum_{s,j} W_{sj} \int_X D_{\alpha_s} f_j(u(\mathbf{x})) \phi(\mathbf{x}) d\mathbf{x} \quad (39)$$

1315 WLOG, assume that $s_1 \neq 0$, and denote $\alpha_{s'} = (s_1 - 1, s_2, \dots, s_p)$. Then, each term in the RHS can
1316 be integrated by parts as

$$1318 \int_X D_{\alpha_s} f_j(u(\mathbf{x})) \phi(\mathbf{x}) d\mathbf{x} = \int_{\mathcal{B}} D_{\alpha_s} f_j(u(\mathbf{x})) \phi(\mathbf{x}) d\mathbf{x} \\ 1319 = - \int_{\mathcal{B}} D_{\alpha_{s'}} f_j(u(\mathbf{x})) D_1 \phi(\mathbf{x}) d\mathbf{x} + \int_{\partial \mathcal{B}} \nu_1 D_{\alpha_{s'}} f_j(u(\mathbf{x})) \phi(\mathbf{x}) d\mathbf{x} \\ 1320 = - \int_{\mathcal{B}} D_{\alpha_{s'}} f_j(u(\mathbf{x})) D_1 \phi(\mathbf{x}) d\mathbf{x}, \quad (40)$$

1324 where D_1 denotes the partial derivative operator w.r.t the first independent variable, and ν_1 is the first
1325 component of the unit outward normal vector.

1326 Repeating this process until all the derivative operations move from $f_j(u)$ to the test function ϕ , we
1327 have

$$1329 \int_X D_{\alpha_s} f_j(u(\mathbf{x})) \phi(\mathbf{x}) d\mathbf{x} = (-1)^{|\alpha_s|} \int_X f_j(u(\mathbf{x})) D_{\alpha_s} \phi(\mathbf{x}) d\mathbf{x} \quad (41)$$

1331 Similarly for the LHS:

$$1333 \int_X D_{\alpha_0} u(\mathbf{x}) \phi(\mathbf{x}) d\mathbf{x} = (-1)^{|\alpha_0|} \int_X u(\mathbf{x}) D_{\alpha_0} \phi(\mathbf{x}) d\mathbf{x} \quad (42)$$

1335 The final optimization problem is to solve for $\mathbf{b} = \mathbf{Gw}$, where \mathbf{w} is the vectorized coefficient matrix
1336 W , and each row in \mathbf{b} and \mathbf{G} is given by computing the integrals in (41) and (42) against a single test
1337 function. The number of rows equals the number of different test functions used.

1339 **Direct integration of symmetry via linear constraints** As we have discussed in Appendix C.2,
1340 we can enforce symmetry by converting it to a set of linear constraints on the parameter W . With this
1341 approach, we can directly incorporate symmetry in weak SINDy. Specifically, we just parameterize
1342 W as in terms of a precomputed basis Q and a trainable vector β and directly substitute this
1343 parameterization of W into the optimization problem of weak SINDy. We adopt this strategy in our
1344 experiments concerning weak SINDy.

1346 **Expressing the equations with differential invariants** The above approach is only possible when
1347 the conditions in Proposition 3.4 about the selected set of symmetry invariants hold. We should
1348 note that it is not always possible to find a set of invariants so that the symmetry condition can be
1349 converted to linear constraints on the parameter W via the procedure in the proof of Proposition 3.4.
One may ask the following question: can we simply express the equations in terms of differential

invariants and apply weak SINDy, similar to Algorithm 2 for the original SINDy formulation? Here, we do not provide a definite conclusion for this question, but only discuss several cases where directly using differential invariants in equations might succeed or fail in weak SINDy.

To adapt to the weak SINDy formulation (38), it is more helpful to consider the symmetry invariants as generated by some fundamental invariants and some invariant differential operators, instead of specifying a complete set of differential invariants for every order. Concretely, there exists a set of invariant differential operators $\{\mathcal{O}_j\}$ and a set of fundamental differential invariants $\mathbf{I} = \{\eta_k\}$ s.t. every differential invariant can be written as $\mathcal{O}_{j_1} \dots \mathcal{O}_{j_n} \eta_k$. For the $\text{SO}(2)$ symmetry group in Example B.5, one possible choice is

$$\eta_1 = \frac{1}{2}(x^2 + y^2), \eta_2 = u, \mathcal{O}_1 = xD_y - yD_x, \mathcal{O}_2 = xD_x + yD_y. \quad (43)$$

We can compose these generating invariant operators to obtain a full library of eligible differential operators up to some order, denoted $\mathbf{D} = \{\mathcal{D}_j\}$. The exact compositions can vary and we can choose the most convenient one for subsequent calculations. For the above $\text{SO}(2)$ example, for up to second-order differential operators, we can choose $\{\mathcal{O}_1, \mathcal{O}_2, \mathcal{O}_1^2, \mathcal{O}_2^2, \frac{2}{\eta_1}(\mathcal{O}_1^2 + \mathcal{O}_2^2)\}$. Note the last operator is exactly the Laplacian.

Then, the complete set of eligible terms (respecting the symmetry) in the equation is $\{\mathcal{D}_j \eta_k : \mathcal{D}_j \in \mathbf{D}, \eta_k \in \mathbf{I}\}$. If we assume, as in SINDy, that the governing equation can be written in linear combination of these symmetry invariants, then we can assign a weight for each $\mathcal{D}_j \eta_k$ and form a coefficient matrix $W = [W_{jk}]$. That is,

$$\mathcal{D}_{j_0} \eta_{k_0} = \sum_{(j,k) \neq (j_0, k_0)} W_{jk} \mathcal{D}_j \eta_k. \quad (44)$$

Then, multiplying each side by a test function $\phi(\mathbf{x})$, we have

$$\int_X \mathcal{D}_{j_0} \eta_{k_0} \phi(\mathbf{x}) d\mathbf{x} = \sum_{(j,k) \neq (j_0, k_0)} W_{jk} \int_X \mathcal{D}_j \eta_k \phi(\mathbf{x}) d\mathbf{x}. \quad (45)$$

The question then boils down to whether we can apply the technique of integration by parts similarly to this set of differential operators and differential functions, since the original algorithm only deals with partial derivative operators D_{α_s} and ordinary functions $f_j(u)$.

To check this, let us explicitly write out the dependency of these operators and fundamental invariants.

Case 1 A relatively simple case is when all invariant operators take the form $\mathcal{D}_j = \sum_s a_s(\mathbf{x}) D_{\alpha_s}$ and $\eta_k = \eta_k(\mathbf{x}, u(\mathbf{x}))$. Each term in the RHS of (45) can be expanded as

$$\begin{aligned} \int_X \mathcal{D}_j \eta_k \phi(\mathbf{x}) d\mathbf{x} &= \sum_s \int_X a_s(\mathbf{x}) D_{\alpha_s} \eta_k(\mathbf{x}, u(\mathbf{x})) \phi(\mathbf{x}) d\mathbf{x} \\ &= \sum_s (-1)^{|\alpha_s|} \int_X \eta_k(\mathbf{x}, u(\mathbf{x})) D_{\alpha_s} [a_s(\mathbf{x}) \phi(\mathbf{x})] d\mathbf{x} \end{aligned} \quad (46)$$

Evaluating (46) does not require estimating partial derivatives of u . Therefore, weak SINDy can be applied to this case quite straightforwardly.

Case 2 However, it is not always possible to have all \mathcal{D}_j as classical linear differential operators and all η_k as ordinary functions. For instance, in Example B.6, there are no ordinary symmetry invariants due to the constraint of translation symmetry.

If we still have linear operators $\mathcal{D}_j = \sum_s a_s(\mathbf{x}) D_{\alpha_s}$, but on the other hand we have differential functions $\eta_k = \eta_k(\mathbf{x}, u^{(n)})$, we can still perform integration by parts as in (46), but the final result becomes

$$\sum_s (-1)^{|\alpha_s|} \int_X \eta_k(\mathbf{x}, u^{(n)}) D_{\alpha_s} [a_s(\mathbf{x}) \phi(\mathbf{x})] d\mathbf{x}, \quad (47)$$

meaning we still have to evaluate whatever partial derivatives remain in η_k . It is possible that we can decrease the order of partial derivatives compared to vanilla sparse regression, but we cannot eliminate all partial derivatives compared to Weak SINDy without any symmetry information.

1404
 1405 **Case 3** The most challenging case is when the invariant differential operators explicitly involve
 1406 the partial derivative, such as $\mathcal{D}_j = \sum_s a_s(\mathbf{x}, u^{(n)}) D_{\alpha_s}$. Then, similar to (47), integration by parts
 1407 yields:

$$1408 \quad \sum_s (-1)^{|\alpha_s|} \int_X \eta_k(\mathbf{x}, u^{(n)}) D_{\alpha_s} [a_s(\mathbf{x}, u^{(n)}) \phi(\mathbf{x})] d\mathbf{x}. \quad (48)$$

1410 In this case, we still need to compute the partial derivatives, not only those in η_k , but also those
 1411 arising from a_s and $D_{\alpha_s}(a_s)$. The latter might involve higher-order derivatives and the benefit of
 1412 using the weak formulation may further diminish.

D ADDITIONAL EXPERIMENT RESULTS

1416 Contents of this section include:

1418

- 1419 • Appendix D.1: Extended results in Table 1 with confidence intervals for the prediction error
 metric over 100 runs.
- 1420 • Appendix D.2: Results for some variants of the sparse regression models considered in
 Table 1.
- 1421 • Appendix D.3: Results for genetic programming-based algorithms under different computa-
 tional budgets.
- 1422 • Appendix D.4: Results for the D-CIPHER (Kacprzyk et al., 2023) baseline and our method
 applied to D-CIPHER on the Darcy flow dataset.
- 1423 • Appendix D.5: Samples of equations discovered by different methods.
- 1424 • Appendix D.6: Visualized prediction errors of equations discovered by different methods.

D.1 RESULTS IN TABLE 1 WITH ERROR ESTIMATES

1432 Table 3: **Extended results in Table 1 with confidence intervals for the prediction error metric over 100**
 1433 **runs. Each table entry is formatted as median [25% quantile, 75% quantile].**

Method		Boussinesq (6)	Darcy flow (7)	Reaction-diffusion (8)
Sparse	PySINDy	0.373 [0.367, 0.380]	-	0.021 [0.020, 0.022]
Regression	SI	0.098 [0.098, 0.098]	-	0.008 [0.007, 0.013]
Genetic	PySR	0.098 [0.098, 0.098]	0.114 [0.089, 0.169]	-
Programming	SI	0.098 [0.098, 0.098]	0.051 [0.031, 0.053]	0.023 [0.015, 0.036]
Transformer	E2E	0.132 [0.109, 0.322]	-	-
	SI	0.104 [0.100, 0.109]	-	-

D.2 VARIANT SPARSE REGRESSION MODELS

1445 Table 4: Results of sparse regression models on the Boussinesq equation and the reaction-diffusion
 1446 system. \mathcal{C} stands for complexity, i.e., the dimensionality of the parameter space. SP stands for success
 1447 probability. The PySINDy and SI rows present the same results as the corresponding rows in Table 1.

Method	Boussinesq (6)		Reaction-diffusion (8)	
	$\mathcal{C} \downarrow$	SP \uparrow	$\mathcal{C} \downarrow$	SP \uparrow
PySINDy	15	0.00	38	0.53
PySINDy*	21	1.00	468	0.00
PySINDy**	15	1.00	198	0.00
SI	13	1.00	28	0.54
SI-aligned	-	-	14	0.56

1456 PySINDy (de Silva et al., 2020; Kaptanoglu et al., 2022) constructs its library θ from a list of variables
 1457 and derivatives, $[\mathbf{u} \parallel \mathbf{u}_\alpha]$ ($|\alpha| > 0$) and a set of scalar functions specified in lambda format. For

example, to include up to quadratic monomial terms in the library, we can specify the following functions: $x \mapsto x$ and $(x, y) \mapsto xy$. However, their original implementation does not allow these functions to be applied to partial derivative terms. As a result, terms such as u_x^2 cannot be modeled. This leads to its failure to discover the Boussinesq equation (6), as we have shown in Table 1.

We modify the implementation and include an additional set of results with different libraries, denoted as PySINDy* in Table 4. The PySINDy* model supports a wider range of library functions, including functions of partial derivatives, e.g., u_x^2 . Further more, we notice that the PySINDy* library while comprehensive, contains many redundant terms, such as interactions between derivatives like $u_x u_{xx}$. Therefore, we implement another library, denoted PySINDy**, where functions such as $(x, y) \mapsto xy$ are only applied when their arguments do not contain at least two different partial derivatives. Therefore, PySINDy** library still includes all the necessary terms to recover the Boussinesq equation but becomes much more compact. A complete description of the hypothesis spaces of different sparse regression-based methods is available in Appendix E.5.

As Table 4 shows, both PySINDy* and PySINDy** succeed in the Boussinesq equation. However, they fail in the reaction-diffusion system because their parameter spaces become too large due to a higher-dimensional total space $X \times U \simeq \mathbb{R}^2 \times \mathbb{R}^2$. Even with the more compact PySINDy**, there are still 198 possible terms for the reaction-diffusion system, and the algorithm never succeeded in 100 runs. This augments the point that SINDy's success relies on an appropriate choice of function library. If the library is too small to contain all the terms appearing in the equation of interest, the discovery is sure to fail. If the library is too large, the optimization problem becomes more difficult in the high-dimensional parameter space. On the other hand, by introducing the inductive bias of symmetry, our method automatically identifies a proper function library that contains all the necessary terms for a PDE with a specific symmetry group, but not other redundant terms.

We include another model in Table 4, SI-aligned, where we derive a set of linear constraints on the sparse regression parameters from the fact that the equations can be expressed in terms of symmetry invariants. In this way, we still optimize the original parameters (though in a constrained subspace) as in the base SINDy model without symmetry, effectively "aligning" the hypotheses about equations from symmetry and the base SINDy model. This method is discussed in detail in Section 3.3 and Appendix C.2. We should also note that this method is mainly developed for incorporating the symmetry constraints into the weak formulation of SINDy. However, it is perfectly acceptable to implement it in the original formulation of SINDy, so we provide its results in Table 4 for reference.

For the reaction-diffusion system, SI-aligned has a 14-dimensional parameter space. The basis for its parameter space is visualized in Figure 5. It achieves a slightly higher success probability than SI (regression with symmetry invariants) and PySINDy (without symmetry information). We do not apply SI-aligned to the Boussinesq equation, because it is not necessary to align the hypotheses from SINDy and symmetry in this case. We can readily convert any equation discovered from SI (regression with symmetry invariants) by multiplying both sides by u_x^2 .

We note that the results on the reaction-diffusion system in Table 4 are for models with the original SINDy formulation, in contrast to the weak SINDy formulation used in Figure 3. Therefore, the results in Figure 3 should not be directly compared to those in Table 1 and Table 4.

D.3 GENETIC PROGRAMMING

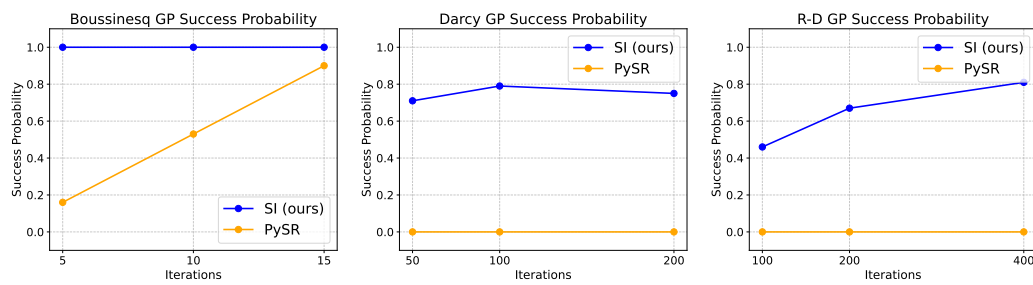


Figure 6: Success Probabilities of GP-based methods on different systems. Our method with symmetry invariants can discover the correct equations with fewer iterations.

1512 For each system in Section 4.1, we run the genetic programming discovery algorithm with three
 1513 different iteration counts, but otherwise keep all hyperparameters constant. In Figure 6, we plot the
 1514 success probability as a function of the iteration count for both the base GP algorithm and our method
 1515 that uses symmetry invariants.

1516 In all cases, we find that using symmetry invariants results in a higher success probability in compar-
 1517 ison to unmodified PySR. Specifically, for the Boussinesq equation, our method achieves a 100%
 1518 chance of discovery with 5 iterations, whereas even with 3 times the number of iterations, PySR only
 1519 yields a 90% success probability. This highlights that using invariants improves the efficiency of
 1520 equation discovery. For Darcy flow and Reaction-Diffusion, we find that the base genetic pro-
 1521 gramming algorithm fails to ever make a correct prediction. On the other hand, using symmetry invariants
 1522 leads to a successful discovery the majority of the time.

1523 We finally note that increasing the number of iterations to 200 for Darcy flow slightly lowers the
 1524 success probability when using symmetry invariants. We hypothesize this is because at higher
 1525 iterations, the search process begins to overfit and introduces extraneous low-order terms. While we
 1526 already drop some terms with small enough coefficients, future works may consider a more refined
 1527 filtration process.

1529 D.4 COMPARISON WITH D-CIPHER

1530 A main advantage of our proposed method is its compatibility with various algorithms for symbolic
 1531 regression. In the main experiments in Section 4.3 in Section 4.4, we have shown that our method
 1532 works well with SINDy (Brunton et al., 2016), weak SINDy (Messenger & Bortz, 2021a), genetic
 1533 programming (Cranmer, 2023), and symbolic transformer (Kamienny et al., 2022). To further
 1534 demonstrate this advantage, we include another base algorithm for symbolic regression, D-CIPHER
 1535 (Kacprzyk et al., 2023), in this section.

1536 Similar to weak SINDy, D-CIPHER (Kacprzyk et al., 2023) uses a variational objective for equation
 1537 discovery. It defines the extended derivative as

$$1539 \mathcal{E}[\mathbf{u}](\mathbf{x}) = a(\mathbf{x})\partial_\alpha h(\mathbf{x}, \mathbf{u}),$$

1540 where a and h are some functions and α is a multi-index indicating partial derivatives. Then, a library
 1541 $\{\mathcal{E}^s\}_{s=1}^S$ of such extended derivatives is specified by the user by providing S triples of (a, α, h) .
 1542 The algorithm then optimizes for a coefficient $\beta \in \mathbb{R}^S$ and a symbolic function $g(\mathbf{x}, \mathbf{u})$ under a
 1543 variational loss and outputs the equation

$$1545 \sum_{s=1}^S \beta^s \mathcal{E}^s[\mathbf{u}](\mathbf{x}) = g(\mathbf{x}, \mathbf{u}).$$

1546 As discussed in Appendix C.3, our approach can be directly used in D-CIPHER to enforce symmetry.
 1547 We demonstrate this with an experiment on the Darcy flow dataset with $\text{SO}(2)$ symmetry. First, we
 1548 obtain the generating invariant operators of $\text{SO}(2)$, i.e. $\mathcal{O}_1 = xD_y - yD_x$ and $\mathcal{O}_2 = xD_x + yD_y$.
 1549 To discover this second-order PDE, we enumerate the following 5 up to second-order differential
 1550 operators composed by \mathcal{O}_1 and \mathcal{O}_2 : $\mathbf{O} = \{\mathcal{O}_1, \mathcal{O}_2, \mathcal{O}_1^2, \mathcal{O}_2^2, \frac{1}{x^2+y^2}(\mathcal{O}_1^2 + \mathcal{O}_2^2)\}$. Note the last operator
 1551 is exactly the Laplacian. On the other hand, we have 2 fundamental differential invariants $x^2 + y^2$
 1552 and u . To enforce symmetry, we replace the manually defined set of extended derivatives $\{\mathcal{E}^s\}$ in
 1553 D-CIPHER by all nontrivial differential functions obtained from applying an operator in \mathbf{O} to one
 1554 of the fundamental differential invariants. Also, instead of searching for general functions of all
 1555 variables (in this case, x, y, u) for the RHS expression, we restrict the search space to functions of
 1556 fundamental differential invariants, i.e. $x^2 + y^2$ and u . Since D-CIPHER uses genetic programming
 1557 to find a free-form expression g , we can simply replace the variable set in genetic programming by
 1558 $\{x^2 + y^2, u\}$ to achieve this.

1559 Table 5 shows the equations discovered by the D-CIPHER baseline and our method. Our method
 1560 can find the correct functional form of the Darcy flow equation, while D-CIPHER with the original
 1561 variables and derivative operators cannot. We comment that the benefit of symmetry is even greater
 1562 here for D-CIPHER than for other SR methods like SINDy, because D-CIPHER requires the user
 1563 to specify both the function coefficient $a(\mathbf{x})$ and the function to be differentiated $h(\mathbf{x}, \mathbf{u})$ for an
 1564 extended derivative. Such choices of functions can be largely arbitrary if no prior knowledge is

1566 Table 5: Discovery results of D-CIPHER-based methods on the Darcy flow dataset. The ground truth
 1567 equation is $8(xu_x + yu_y) - (u_{xx} + u_{yy}) - e^{4(x^2+y^2)} = 0$.
 1568

Method	Discovered equation
D-CIPHER	$xu_x + yu_y - 2.09xu_y - 2.09yu_x - 0.19u_y = 7.98x^2y^2 + 2.51xy + 0.80$
D-CIPHER-SI (ours)	$(xu_x + yu_y) - 0.13(u_{xx} + u_{yy}) = 0.13e^{4.12(x^2+y^2)}$

1572
 1573 available. On the other hand, our symmetry-based approach automatically selects this dictionary of
 1574 differential functions.
 1575

1577 D.5 SAMPLES OF DISCOVERED EQUATIONS

1579 In Table 6, we list some randomly selected equations discovered by different methods for the
 1580 Boussinesq equation (6). Some methods almost consistently discover correct/incorrect equations (i.e.,
 1581 have success probabilities close to 1 or 0), so we only select one sample for each. For other methods
 1582 with a large variance in the discovered equations, we display two samples: a correct equation and an
 1583 incorrect one.

1584 The ground truth equation in the original variables is given in (6). The ground truth equation in the
 1585 symmetry invariants is given by

$$\eta_{(0,2)} + \eta_{(0,0)}\eta_{(2,0)} + \eta_{(4,0)} + 1 = 0 \quad (49)$$

1589 Table 6: Samples of discovered equations from the observed solution of the Boussinesq equation
 1590 (6). For GP-based methods, we include results from different numbers of iterations (indicated by " N
 1591 its"). For transformer-based methods, we include two samples for each method because of the large
 1592 variance of discovered equations from different runs.
 1593

Method	Equation sample(s)
Sparse regression	$u_{tt} = -1.01u_{xxxx} - 0.79uu_{xx}$
	$u_{tt} = -1.01u_{xxxx} - 0.99u_x^2 - 0.98uu_{xx}$
	$\eta_{(0,2)} = -1.00 - 1.00\eta_{(4,0)} - 1.00\eta_{(0,0)}\eta_{(2,0)}$
Genetic programming	$uu_{xx} + 1.00u_{tt} + u_{xxxx} = 0$
	$uu_{xx} + u_{tt} + u_x^2 + 1.00u_{xxxx} = 0$
	$1.00\eta_{(0,0)}\eta_{(2,0)} + 1.00\eta_{(0,2)} + 1.00\eta_{(4,0)} + 1 = 0$
Transformer	$(1) u_{tt} = -1.13uu_{xx} - 0.98u_{xxxx} - 0.30 u_x $
	$(2) u_{tt} = -0.85uu_{xx} - 0.75u_x^2 - 0.99u_{xxxx}$
	$(1) \eta_{(0,2)} = -1.05\eta_{(0,0)}\eta_{(2,0)} - 1.00\eta_{(4,0)} - 0.96$
	$(2) \eta_{(0,2)} = -0.81\eta_{(0,0)}\eta_{(2,0)} - 0.40\eta_{(0,0)} - 0.98\eta_{(4,0)} - 0.90$

1606 Table 7 lists the equation samples discovered from the Darcy flow dataset. The ground truth equation
 1607 in original variables is given in (7), and the ground truth equation in symmetry invariants is given by
 1608

$$8\zeta_2 - \Delta u - e^{4R^2} = 0, \quad (50)$$

1609 where $\zeta_2 = xu_x + yu_y$, $\Delta u = u_{xx} + u_{yy}$, and $R^2 = x^2 + y^2$ are among the rotational invariants
 1610 used in symbolic regression.
 1612

1613 Table 7: Samples of discovered equations for the Darcy flow dataset.
 1614

Method	Equation sample
Genetic programming	$u - 0.47x^2y^2 - 0.38e^{0.09(u_{xx}+u_{yy})} + 0.20 = 0$
Transformer	$\zeta_2 - 0.13\Delta u - 0.13e^{4.01R^2} = 0$
E2E	$u_{xx} = -7.43\sqrt{u^2 + 0.65u_x^2}$
SI	$\Delta u = -2.56u + 0.85\zeta_2 + 0.29$

Finally, Table 8 lists the equation samples discovered from the reaction-diffusion dataset. The ground truth equation in original variables is given in (8) with $d_1 = d_2 = 0.1$, and the ground truth equation in symmetry invariants is given by

$$\begin{aligned} I_t &= 0.1(I_{xx} + I_{yy}) + A(1 - A) \\ E_t &= 0.1(E_{xx} + E_{yy}) - A^2 \end{aligned} \quad (51)$$

where $I_\mu = uu_\mu + vv_\mu$ and $E_\mu = -vu_\mu + uv_\mu$ for any multiindex μ of t, x, y , and $A = u^2 + v^2$.

Table 8: Samples of discovered equations for the reaction-diffusion system dataset. Each discovered result contains two equations, since this is an evolution system with two dependent variables u, v .

Method	Equation sample
PySINDy	$\begin{cases} u_t = 0.96u - 0.97u^3 + 1.00^3 - 0.97uv^2 + 1.00u^2v + 0.09u_{xx} + 0.09u_{yy} \\ v_t = 0.96v - 1.00u^3 - 0.97v^3 - 1.00uv^2 - 0.96u^2v + 0.09v_{xx} + 0.09v_{yy} \end{cases}$
Sparse regression	$\begin{cases} u_t = 0.21u - 0.24u^3 + 1.00v^3 - 0.23uv^2 + 0.99u^2v \\ v_t = 0.21v - 1.01u^3 - 0.24v^3 - 0.99uv^2 - 0.23u^2v \end{cases}$
SI	$\begin{cases} I_t = 0.10I_{xx} + 0.10I_{yy} + 0.96A - 0.96A^2 \\ E_t = 0.10E_{xx} + 0.10E_{yy} - 1.00A^2 \end{cases}$
SI-aligned	$\begin{cases} u_t = 0.95u - 0.96u^3 + 1.00v^3 - 0.96uv^2 + 1.00u^2v + 0.09u_{xx} + 0.09u_{yy} \\ v_t = 0.95v - 1.00u^3 - 0.96v^3 - 1.00uv^2 - 0.96u^2v + 0.09v_{xx} + 0.09v_{yy} \end{cases}$
Genetic programming	$\begin{cases} u_t = 0.92v \\ v_t = -0.92u \end{cases}$
SI	$\begin{cases} I_t = 0.10I_{xx} + 0.10I_{yy} + A - 1.00A^2 \\ E_t = 0.10E_{xx} + 0.10E_{yy} - 1.00A^2 \end{cases}$
Transformer	$\begin{cases} u_t = 0.89u_y \\ v_t = -0.91u \end{cases}$
SI	$\begin{cases} I_t = 0 \\ E_t = 0.50 \arctan(0.45E_y - 0.31E_y/(-540.12AE_y + \dots) + \dots) + \dots \end{cases}$

D.6 PREDICTION ERRORS OF DISCOVERED EQUATIONS

In Table 1, we report the prediction errors of the discovered equations on the three PDE systems. Specifically, for the Boussinesq equation and the reaction-diffusion system, we simulate the discovered PDE from an initial condition for a certain time period, e.g., $t \in [0, 20]$ for the Boussinesq equation and $t \in [0, 10]$ for the reaction-diffusion system. Then, we compare the numerical solution with the ground truth solution from the same initial condition at the end of the time period.

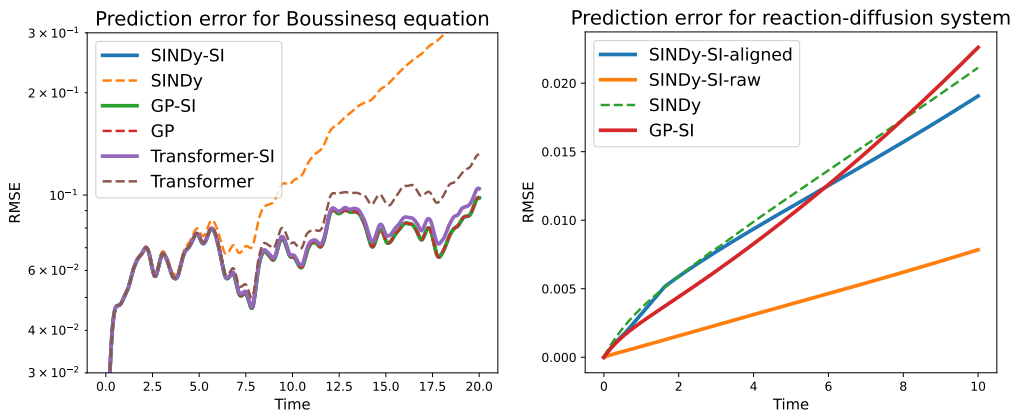


Figure 7: Prediction error over time using the discovered equations.

In addition to the prediction error at the end of the simulation time, Figure 7 shows the errors at each simulation timestep. We do not include methods whose error curves grow too fast due to the

incorrectly identified equations. The results in Figure 7 are consistent with those in Table 1. Generally, the discovered equations with smaller prediction errors at the end of the simulation time also have lower prediction errors throughout the entire time interval.

For Darcy flow (7), since it describes the steady state of a system and does not involve time derivatives, we do not simulate the discovered PDEs. Instead, we evaluate each discovered PDE $F(\mathbf{x}, u^{(n)}) = 0$ on the test dataset $\{(\mathbf{x}, u^{(n)}): \mathbf{x} \in \Omega\}$ and report the residual as the prediction error. In addition to the average error over all the spatial grid points reported in Table 1, we visualize the error heatmaps over the grid in Figure 8. It can be observed that the discovered equations with symmetry invariants have lower errors across the entire grid.

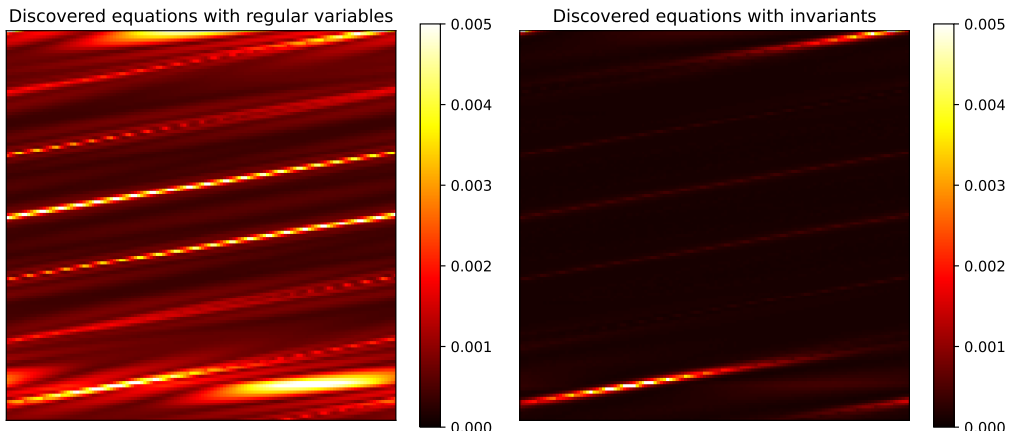


Figure 8: Prediction error of discovered equations from genetic programming methods for Darcy flow. Left: genetic programming with regular variables. Right: genetic programming with symmetry invariants.

E EXPERIMENT DETAILS

In this section, we describe the experiment setups required to reproduce the experiments. In terms of computational resources, our experiments are conducted with 12 INTEL(R) XEON(R) PLATINUM 8558 CPUs and should be reproducible within minutes with any modern CPUs.

E.1 DATA GENERATION

Boussinesq equation The equation is solved using a Fourier pseudospectral method for spatial derivatives and a fourth-order Runge-Kutta (RK4) scheme for time integration. The solution is computed on a periodic spatial domain $[-L, L]$ with $N = 256$ grid points. The equation is reformulated as a first-order system in time by introducing $v = u_t$, and both u and v are evolved in time. Spatial derivatives are computed using the Fast Fourier Transform, and time derivatives of u up to the fourth order are derived analytically from the governing equation. At each time step, values of u are recorded in the dataset for equation discovery. The simulation starts from an initial condition of $u(x) = 0.5e^{-x^2}$ and $u_t = 0$ and proceeds up to a final time $T = 20$ with a time step of $\Delta t = 0.001$. Starting from the solution at $T = 20$, we simulate for another $T' = 20$ with the same configuration to obtain a test dataset for evaluating prediction errors of the discovered equations.

Darcy flow We use the data generation code² from PDEBench (Takamoto et al., 2022) to generate the steady-state solution of Darcy flow over a unit square. The solution is obtained by numerically solving a temporal evolution equation

$$u_t(\mathbf{x}, t) - \nabla(a(\mathbf{x}) \nabla u(\mathbf{x}, t)) = f(x), \mathbf{x} \in (-0.5, 0.5)^2, \quad (52)$$

with $a(\mathbf{x}) = e^{-4\|\mathbf{x}\|_2^2}$ and $f(\mathbf{x}) = 1$

²https://github.com/pdebench/PDEBench/tree/main/pdebench/data_gen/data_gen_NLE/ReactionDiffusionEq

1728
 1729 **Reaction-diffusion** We use the data generation code³ from PySINDy (de Silva et al., 2020; Kap-
 1730 tanoglu et al., 2022). The spatial domain is $[-10, 10] \times [-10, 10]$ with 128 grid points in each
 1731 direction. The simulation proceeds up to a final time $T = 10$ with a time step $\Delta t = 0.05$. We perturb
 1732 the numerical solution by a 0.05% noise and record the values of u, v to the dataset for equation
 1733 discovery. Starting from the solution at $T = 10$, we simulate for another $T' = 10$ with the same
 1734 configuration to obtain a test dataset for evaluating prediction errors of the discovered equations.

1735 **E.2 SPARSE REGRESSION**
 1736

1737 **Boussinesq equation** For SINDy with original variables, we fix u_{tt} as the LHS of the equation
 1738 and include functions of up to 4th-order derivatives on the RHS. For PySINDy in Table 1, the library
 1739 contains monomials on $U^{(4)}$ with degree in u no larger than 2 and degree in any partial derivative
 1740 terms u_α no larger than 1. For example, $u^2 u_x$ is included, but u^3, u_x^2 are not. For PySINDy*, the
 1741 library contains all monomials on $U^{(4)}$ up to degree 2. For example, u_x^2 and uu_x are included. Note
 1742 that the PySINDy* library does not contain all functions in the original PySINDy library, e.g., $u^2 u_x$
 1743 is not included because it has degree 3.

1744 Our method, SI, uses the invariant set in Example B.6 for sparse regression. Specifically, $\eta_{(0,2)} =$
 1745 u_{tt}/u_x^2 is used as the LHS of the equation, and the rest of the invariants are included in the RHS.
 1746 The function library contains all monomials of these RHS invariants up to degree 2. Also, since the
 1747 invariants contain rational functions with u_x on the denominator, we remove the data points with
 1748 $|u_x| < 0.1$ to avoid numerical issues.

1749 We also conduct an additional experiment to investigate the impact of the threshold value for $|u_x|$. In
 1750 Table 9, we enumerate different threshold values from $\{0.0001, 0.001, 0.01, 0.1, 0.2, 0.3\}$, and report
 1751 the resulting filtered dataset sizes (and their proportions compared to the unfiltered dataset), and the
 1752 success probability (SP) and the prediction error (PE) metrics as in Table 1.

1753 First of all, we notice that when the threshold value is small ($c = 0.0001$), i.e. effectively no filtering,
 1754 the success probability for SINDy using invariant functions dramatically decreases. This exactly
 1755 shows the necessity of applying this numerical filter, as u_x values close to zero would cause the
 1756 invariant features to have large magnitudes and make the SINDy optimization unstable.

1757 Then, as we increase c , we observe that our method can achieve 100% success probability for
 1758 $c \in \{0.001, 0.01, 0.1\}$, showing its robustness to different choices of the threshold to some extent.
 1759 When we further increase c , the filtered dataset becomes much smaller, and the success probability
 1760 decreases. However, even with $c = 0.3$ and only 99 data points, our method is still able to recover
 1761 the correct equation with more than 50% probability.

1762
 1763
 1764 Table 9: SINDy with invariant functions on the Boussinesq equation when removing data points with
 1765 $|u_x| < c$ for different threshold values c . In the second row, we report the number of samples in the
 1766 filtered datasets and their proportions compared to the original dataset. The success probability (SP)
 1767 and the prediction error (PE) are computed from 100 runs with different random seeds, in the same
 1768 way as Table 1. The prediction error is reported as median [25% quantile, 75% quantile].

Threshold c	Dataset size	SP	PE
0.0001	99,756 (97.4%)	0.36	NaN [0.129, NaN]
0.001	97,956 (95.7%)	1.00	0.103 [0.099, 0.118]
0.01	85,591 (83.6%)	1.00	0.098 [0.098, 0.099]
0.1	26,231 (25.6%)	1.00	0.098 [0.098, 0.098]
0.2	1,318 (1.3%)	0.91	0.098 [0.097, 0.108]
0.3	99 (0.1%)	0.52	0.100 [0.098, NaN]

1777 For all methods, we flatten the data on the spatiotemporal grid and randomly sample 2% of the data
 1778 for each run. The data filtering process in SI-raw is performed after subsampling. The threshold value
 1779 for sequential thresholding is set to 0.25, and the coefficient for L_2 regularization is set to 0.05.

1780
 1781 ³https://github.com/dynamicslab/pysindy/blob/master/examples/10_PDEFIND_examples.ipynb

Darcy flow Sparse regression-based methods are not directly applicable to Darcy flow (7) because there exist terms such as $e^{-4(x^2+y^2)}$. While it is still possible to include all necessary terms in the function library so that the equation can be written in the linear combination form (4), the knowledge of these complicated terms is nontrivial and should not be assumed available before running the equation discovery algorithm.

Reaction-Diffusion For SINDy with original variables, We fix u_t and v_t as the LHS of the equation and include functions of up to 2nd-order spatial derivatives on the RHS. In PySINDy, the library contains monomials of u, v up to degree 3 and all spatial derivatives up to order 2. In PySINDy*, the library contains all monomials of u, v and their up to second-order spatial derivatives up to degree 3.

Our method uses the invariant set $\{t, x, y, u^2 + v^2\} \cup \{\mathbf{u} \cdot \mathbf{u}_\mu\} \cup \{\mathbf{u}^\perp \cdot \mathbf{u}_\mu\}$, where $\mathbf{u} = (u, v)^T$ and μ is a multiindex of t, x, y . We will denote $I_\mu = \mathbf{u} \cdot \mathbf{u}_\mu$ and $E_\mu = \mathbf{u}^\perp \cdot \mathbf{u}_\mu$. We use I_t and E_t as the LHS of the equation, and the rest of the invariants are included in the RHS. The function library contains all monomials of these RHS invariants up to degree 2.

We randomly sample 10% of the data for each run. The threshold value for sequential thresholding is set to 0.05. The coefficient for L_2 regularization is set to 0 for SINDy with original variables and 0.1 for our method with symmetry invariants.

For the experiments with different levels of noise (Section 4.4), we use weak SINDy as the base algorithm. We use the implementation of weak SINDy from the PySINDy package (Kaptanoglu et al., 2022). The function library is the same as SINDy as described above. To enforce symmetry, instead of directly using the symmetry invariants, we derive a set of linear constraints on the sparse regression parameters to adapt to weak SINDy. This procedure is further described in Appendix C.3.

E.3 GENETIC PROGRAMMING

In all experiments, to determine if an equation matches the ground truth we first expand the prediction into a sum of monomial terms. We then eliminate all terms whose relative coefficient is below 0.01. For each term in the filtered expression, we see if it matches any term in the ground truth expression. This is done by randomly sampling 100 points from the standard normal distribution and evaluating both the prediction and candidate ground truth term on the generated points. Note that we drop the coefficients before evaluation. If all evaluations of the predicted term have a relative error of less than 5% from those of the ground truth, the terms are said to match. If there is a perfect matching between the terms in the ground truth and prediction, the prediction is listed as correct.

Rather than directly returning a single equation, PySR finally produces a hall-of-fame that consists of multiple candidate solutions with varying complexities. To finally pick a single prediction, we use a selection strategy equivalent to the “best” option from PySR.

Boussinesq equation For the Boussinesq equation (6), we first randomly subsample 10000 datapoints. We configure PySR to use the addition and multiplication operators, to have 127 populations of size 27, and to have the default fraction-replaced coefficient of 0.00036.

When running with ordinary variables, we sequentially try fixing the LHS to each variable in $(\mathbf{x}, u^{(4)})$ and allow the RHS to be a function of all remaining variables. Similarly, runs using invariants sequentially fix the LHS from the set given by Example B.6 and the RHS as a function of all other invariants.

For each iteration count of 5, 10, and 15, we run the algorithm using invariant or ordinary variables and report the number of correct predictions out of 100 trials.

Darcy flow In the Darcy experiment (7), we eliminate all points that are within 3 pixels from the border and then randomly subsample 10000 datapoints. We configure PySR to use the addition, multiplication, and exponential operators; to have 127 populations of size 64; and to have a fraction-replaced coefficient of 0.1. We further constrain it to disallow nested exponentials (e.g. $\exp(\exp(x) + 4)$).

1836 We try all possible ordinary variables in $(\mathbf{x}, u^{(2)})$ for the LHS and the RHS is then a function of the
 1837 unused variables. Likewise when using invariants, we fix the LHS to each possible invariant specified
 1838 in Example B.5 and set the RHS as a function of the remaining invariants.

1839 For each iteration count of 50, 100, and 200, we run the algorithm using invariant or ordinary variables
 1840 and report the number of correct predictions out of 100 trials.

1842 **Reaction-Diffusion** For the Reaction Diffusion equation (8), we remove all points that are within 3
 1843 pixels from the border or have timestamp greater than or equal to 40, and then randomly subsample
 1844 10000 datapoints. We configure PySR to use the addition and multiplication operators, to have 127
 1845 populations of size 64, and to have a fraction-replaced coefficient of 0.5.

1846 In the ordinary variable case, we fix the LHS as either u_{tt} or v_{tt} and allow the RHS to be a function
 1847 of all other variables in $(\mathbf{x}, u^{(2)})$. When using invariants, the LHS is fixed to be either I_t or E_t and
 1848 the RHS is then a function of all remaining invariants.

1849 For each iteration count of 100, 200, and 400, we run the algorithm using regular and ordinary
 1850 variables and report the number of correct predictions out of 100 trials.

1852

1853 E.4 SYMBOLIC TRANSFORMER

1854 We use the pretrained symbolic transformer model provided in the official codebase⁴ from Kamienny
 1855 et al. (2022). The transformer-based symbolic regressor is initialized with 200 maximal input points
 1856 and 100 expression trees to refine. The variable sets used in the symbolic transformer are the same as
 1857 those described in the genetic programming experiments, except for the Boussinesq equation, where
 1858 we remove all mixed derivative terms in both the original variable set and the symmetry invariant set.
 1859 We find that the symbolic transformer can sometimes discover the correct equation under this further
 1860 simplified setup, but fails when using the larger variable sets.

1861 We also fix the LHS of the function and use the remaining variables as RHS features. For the
 1862 Boussinesq equation, the LHS is fixed to u_{tt} for original variables and $\eta_{(0,2)}$ for symmetry invariants.
 1863 For the Darcy flow, the LHS is fixed to u_{xx} for original variables and Δu for symmetry invariants.
 1864 For the reaction-diffusion system, the LHS is fixed to u_t, v_t for original variables and I_t, E_t for
 1865 symmetry invariants.

1866

1867 E.5 HYPOTHESIS SPACES OF EQUATION DISCOVERY ALGORITHMS

1868 Table 10 and Table 11 describe the hypothesis spaces of different equation discovery algorithms when
 1869 applied to the Boussinesq equation and the reaction-diffusion system.

1870

1871 Table 10: Hypothesis spaces of different equation discovery algorithms for the Boussinesq equation.

Method		Hypothesis space
PySINDy		$u_{tt} = W\theta(u^{(4)}), \{\theta^j\} = \{ab : a \in \text{Mono}_{\leq 2}(U), b \in \{1, u_x, \dots, u_{xxxx}\}\}$
Sparse	PySINDy*	$u_{tt} = P(u^{(4)}) \in \text{Poly}_{\leq 2}(U^{(4)})$
Regression	PySINDy**	$u_{tt} = W\theta(u^{(4)}), \{\theta^j\} = \{u^{c_0} u_1^{c_1} u_2^{c_2} u_3^{c_3} u_4^{c_4} : c_i \geq 0, \sum_0^4 c_i \leq 2, \sum_1^4 \text{sgn}(c_i) \leq 1\}$
	SI	$\eta_{(0,2)} = P(\eta) \in \text{Poly}_{\leq 2}(\{\eta_{(\alpha,\beta)}\} \setminus \{\eta_{(0,2)}\})$
Genetic	PySR	$z^j = f(\mathbf{z}^{-j})$ for $\mathbf{z} = (\mathbf{x}, u^{(4)})$ and some j
Programming	SI	$\eta_{(\alpha_0, \beta_0)} = f(\eta_{-(\alpha_0, \beta_0)})$ for $\eta = \{\eta_{(\alpha, \beta)} : \alpha + \beta \leq 4\}$ and some (α_0, β_0)

1881

1882 DECLARATION OF LLM USAGE

1883

1884 We used LLM solely to assist with minor language editing and polishing of the manuscript text. LLM
 1885 was not involved in the research design, experiments, analysis, or in generating any original scientific
 1886 content.

1887

1888

1889

⁴<https://github.com/facebookresearch/symbolicregression/blob/main/Example.ipynb>

1890
 1891
 1892
 1893
 1894
 1895
 1896
 1897
 1898
 1899
 1900
 1901
 1902
 1903
 1904
 1905
 1906
 1907
 1908
 1909
 1910

1911 Table 11: Hypothesis spaces of different equation discovery algorithms for 2D reaction-diffusion.
 1912 $\mathbf{u}^{(n)} \in U^{(n)}$ denotes the collection of all up to n th order *spatial* derivatives. $\alpha = [\alpha_1, \alpha_2]$ is the
 1913 multiindex for spatial variables. $\mathbf{x} = (x, y, t)$. $A = u^2 + v^2$.

	Method	Hypothesis space
1916	PySINDy	$\mathbf{u}_t = W\theta(\mathbf{u}^{(2)}), \{\theta^j\} = \text{Mono}_{\leq 3}(U) \bigcup \{\mathbf{u}_\alpha : \alpha \leq 2\}$
1917	Sparse PySINDy*	$\mathbf{u}_t = P(\mathbf{u}^{(2)}) \in \text{Poly}_{\leq 3}(U^{(2)})$
1918	Regression PySINDy**	$\mathbf{u}_t = W\theta(\mathbf{u}^{(2)}), \{\theta^j\} = \{\prod_{i,\alpha} (u_\alpha^i)^{c_\alpha^i} : \sum c_\alpha^i \leq 3, \sum_{ \alpha \geq 1} \text{sgn}(c_\alpha^i) \leq 1\}$
1919	SI	$[I_t, E_t]^T = P \in \text{Poly}_{\leq 2}(A, \mathbf{x}, I_\alpha, E_\alpha; \alpha \leq 2)$
1920	SI-aligned	$\mathbf{u}_t = W\theta(\mathbf{u}^{(2)}), W^{jk} = Q^{ijk} \beta^i$ for some precomputed Q
1921	Genetic Programming	$\mathbf{u}_t = \mathbf{f}(\mathbf{x}, \mathbf{u}^{(2)})$
1922	PySR	$[I_t, E_t]^T = \mathbf{f}(A, \mathbf{x}, I_\alpha, E_\alpha; \alpha \leq 2)$

1924
 1925
 1926
 1927
 1928
 1929
 1930
 1931
 1932
 1933
 1934
 1935
 1936
 1937
 1938
 1939
 1940
 1941
 1942
 1943